Vol. 92 No. 5 pp. 1700–1727 ACTA GEOLOGICA SINICA (English Edition) Oct. 2018

Neoproterozoic–Early Paleozoic Tectonic Evolution of the South China Craton: New Insights from the Polyphase Deformation in the Southwestern Jiangnan Orogen

ZHAO Zhongbao[1, 2, *], XU Zhiqin[3], MA Xuxuan[1, 2], LIANG Fenghua[1, 2] and GUO Peng[4]

1 *Key Laboratory of Deep-Earth Dynamics of Ministry of Natural Resources, China*
2 *Institute of Geology, Chinese Academy of Geological Sciences, Beijing 100037, China*
3 *State Key Laboratory for Mineral Deposits Research, Department of Earth Sciences, Nanjing University, Nanjing 210046, China*
4 *School of Earth Science and Resources, China University of Geosciences, Beijing 100083, China*

Abstract: A >1500–km–long northeast–southwest trending Neoproterozoic metamorphic belt in the South China Craton (SCC) consists of subduction mélange and extensional basin deposits. This belt is present under an unconformity of Devonian–Carboniferous sediments. Tectonic evolution of the Neoproterozoic rocks is crucial to determining the geology of the SCC and further influences the reconstruction of the Rodinia supercontinent. A subduction mélange unit enclosed ca.1000–850–Ma mafic blocks, which defined a Neoproterozoic ocean that existed within the SCC, is exposed at the bottom of the Jiangnan Orogen (JO) and experienced at least two phases deformation. Combined with new (detrital) zircon U–Pb ages from metasandstones, as well as igneous rocks within the metamorphic belt, we restrict the strongly deformed subduction mélange as younger than the minimum detrital age ca. 835 Ma and older than the ca. 815 Ma intruded granite. Unconformably overlying the subduction mélange and the intruded granite, an intra–continental rift basin developed <800 Ma that involved abundant mantle inputs, such as mafic dikes. This stratum only experienced one main phase deformation. According to our white mica $^{40}Ar/^{30}Ar$ data and previously documented thermochronology, both the Neoproterozoic mélange and younger strata were exhumed by a 490–400–Ma crustal–scale positive flower structure. This orogenic event probably induced the thick–skinned structures and was accompanied by crustal thickening, metamorphism and magmatism and led to the closure of the pre–existing rift basin. Integrating previously published data and our new results, we agree that the SCC was located on the periphery of the Rodinia supercontinent from the Neoproterozic until the Ordovician. Furthermore, we prefer that the convergence and dispersal of the SCC were primarily controlled by oceanic subduction forces that occurred within or periphery of the SCC.

Key words: Rodinia supercontinent, South China Craton, Jiangnan Orogen, intra–continental rifting, intra–continental orogen

1 Introduction

Repeated cycles of supercontinent amalgamation and dispersal through plate tectonics have a profound influence on the evolution of Earth's crust, atmosphere, hydrosphere and life through the present (Nance et al., 2014; Cawood et al., 2016). Spatiotemporal relationships of different fragments from historical supercontinents are key to understanding these influences (Collins and Pisarevsky, 2005; Li et al., 2008). Particularly, due to the rearrangement and continued tectonic evolution of these fragments, the Precambrian supercontinental evolution and its related geodynamics, such as the Rodinia supercontinent, are still debated (Li et al., 2008; Zhao and Cawood, 2012; Cawood et al., 2013).

The South China Craton (SCC) once belonged to part of the Rodinia supercontinent and is a critical piece for the Rodinia paleogeographic reconstruction (Li et al., 2008;

* Corresponding author. E-mail: zhaozhb04@163.com

© 2018 Geological Society of China

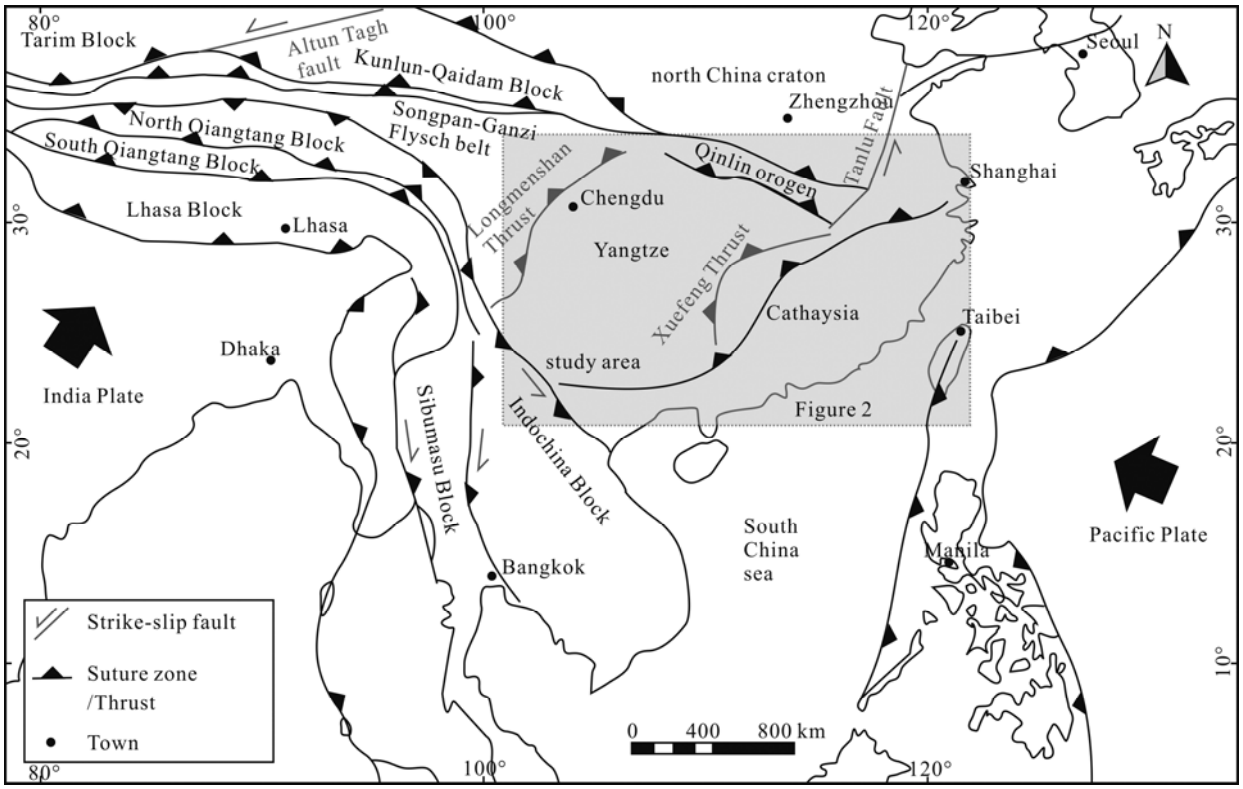


Fig. 1. Simplified regional structural map of Southeast Asia, showing the location of the South China Craton (SCC) and its tectonic subdivision, which was modified from Li et al. (2016d) and Faure et al. (2016).
The SCC is surrounded by the North China Craton and Kunlun–Qaidam to the north, the Tibetan Plateau and Sibumasu–Indochina Block to the south-west, and the Pacific plate to the east. The SCC includes the Songpan–Ganzi Flysch belt, Yangtze Block and Cathaysia Block. The black arrows show the directions of the Pacific and India Plate drift. Figure 2 is highlighted by a gray shadow.

Cawood et al., 2013). Traditionally, the SCC consists of the Yangtze and Cathaysia Blocks and the Neoproterozoic Jiangnan Orogen (JO) located between them (Figs. 1–2) (Charvet, 2013), which record the Rodinia convergence and dispersal (Zheng et al., 2008; Zhao, 2015). However, 1) when the SCC finally amalgamated and 2) where the SCC was located during the amalgamation and dispersal of Rodinia, whether it was internal or on the periphery, is still debated (Li et al., 2002; Li et al., 2003; Wang et al., 2007; Li et al., 2008; Cawood et al., 2013; Charvet, 2013; Cui et al., 2015).

Another open controversy is the geological significance of a suite of Late Neoproterozoic strata in the SCC, known as the Danzhou Group (or its equivalent strata) (Yang et al., 2015; Yao et al., 2015a). The Late Neoproterozoic strata are thought to have been deposited in an intra–continental rift basin formed either by a 'plume–rift' model (Li et al., 2003; Wang and Li, 2003; Zheng et al., 2007; Zheng et al., 2008) or a 'slab–arc' model (Zhou et al., 2002; Zhou et al., 2006; Zhao et al., 2011). The 'plume–rift' model proposes that the upwelling of a super plume triggered major magmatism after 850 Ma in the SCC and assumes that the rising super plume lead to the breakup of Rodinia (Li et al., 1999; Li et al., 2002; Li et al., 2003; Li et al., 2008; Wang et al., 2011). Nonetheless, the 'slab–arc' model argues that the Late Neoproterozoic strata were deposited in the intra–continental rifted Nanhua Basin between 820 and 730 Ma, and probably reflect backarc spreading above the long–lived (950–735 Ma) oceanic subduction zone along the northwestern margin of the Yangtze Block (Fig. 2) (Zhou et al., 2002; Zhou et al., 2006; Zhao et al., 2011).

According to the above discussions, the Neoproterozoic–Early Paleozoic tectonic evolution of the SCC remains poorly confined, precluding construction of a rational geodynamic model. This paper focuses on the composition, macro– and microstructures, and geochronology of the deformation history of the Neoproterozoic subduction–related mélange, as well as the unconformably–overlying strata in the Yuanbaoshan region, located in the southwestern JO, northern Guangxi Province (China). Three new 3D structural profiles were reconstructed based on field data, that, together with age constraints from recently published and our new data, allow us to propose a more detailed tectonic evolution model of the JO.

2 Geological Setting

From the northwest to the southeast, the SCC consists

of the Yangtze and Cathaysia Blocks, which are separated by the Jiangnan Orogen (Fig. 1) (Zhai, 2015; Zhao, 2015). Both the north and south SCC are confined by Triassic suture zones, and the Pacific Plate lies to the east (Fig. 1) (Faure et al., 2016; Li et al., 2016a). The Yangtze Block exposes Archean–Paleoproterozoic gneissic basement in its core (Wang et al., 2010; Wang et al., 2013c) and the Meso–to–Neoproterozoic subduction–related complex surrounds its edge (Fig. 2) (Zhou et al., 2006; Zhao and Cawood, 2012). Weakly–metamorphosed Neoproterozoic strata and unmetamorphosed Cryogenian–Ediacaran unconformably overlie old metamorphic rocks (Wang and Li, 2003; Zhang et al., 2016b). The Cathaysia Block comprises Paleoproterozoic (1.8–2.0 Ga) to Neoproterozoic basement rocks, which contain gneisses, amphibolites, and migmatite (Fig. 2) (Zhao and Cawood, 2012; Dong et al., 2015). Neoproterozoic volcanic–sedimentary rocks cover a large area of the Cathaysia Block (Fig. 2) (Shu, 2012), some of which experienced high greenschist to amphibolite facies metamorphism (Wang et al., 2012b).

Between the Yangtze Block to the northwest and the Cathaysia Block to the southeast, lies the NE–trending, >1500–km–long JO (Fig. 2) (Lin et al., 2015; Zhang and

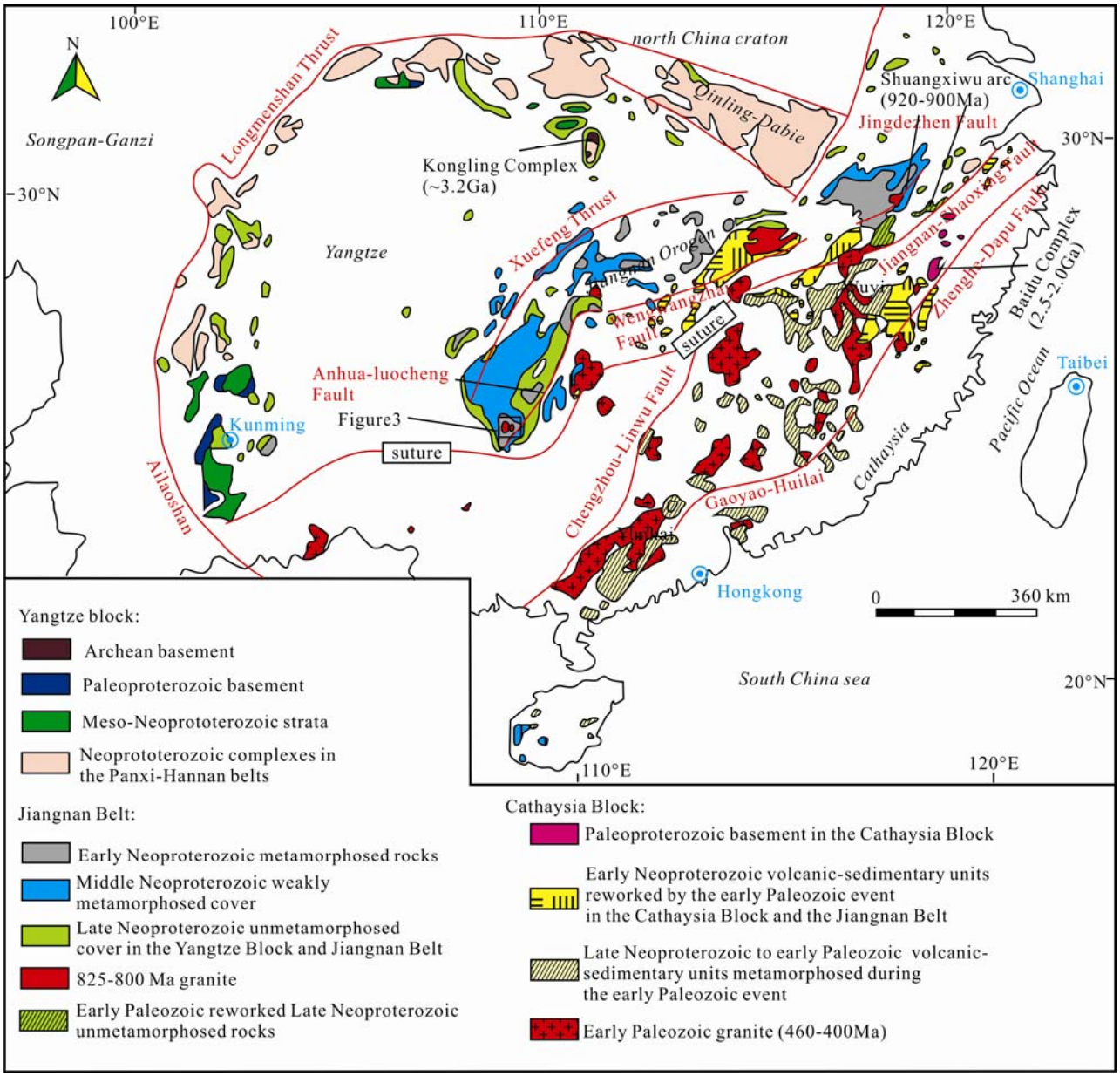


Fig. 2. Simplified geological map of the South China Craton, including the Yangtze Block, the Jiangnan Orogen and the Cathaysia Block.

Primarily Precambrian strata and the Early Paleozoic igneous intrusion are included in this figure. This figure was modified from Zhao and Cawood (2012), Dong et al. (2015) and Yu et al. (2016). The scope of Figure 3 is shown by the black frame.

Wang, 2016). Relics of the ocean between the Yangtze and Cathaysia Blocks may be as old as the Paleoproterozoic (ca. 2.0–1.9 Ga) (Dong et al., 2015). However, the core of the JO has Neoproterozic mélange and strata, whereas Cambrian to Cenozoic sediments are located on the two wings (Zhao and Cawood, 2012; Wang et al., 2013b).

After ca. 820 Ma, both the JO and Cathaysia Block experienced extension and rifting, forming the Nanhua Basin, in which thick flysch and intercalated bimodal volcanic layers with ~825–780 Ma ages (Wang and Li, 2003; Zheng et al., 2008) were deposited. A littoral–neritic depositional environment prevailed in the Cambrian and turned into a neritic–bathyal setting during the Early–Middle Ordovician (Shu, 2012; Shu et al., 2014; Zhang et al., 2016b). Shu et al. (2014) attributed the depositional sequence transition from neritic–bathyal to littoral–land environment to the initial uplift in the Cathaysia Block during the Late Ordovician. The abovementioned strata are overlain unconformably by Devonian conglomerate (Xun et al., 1996; Chen et al., 2016).

2.1 Mapped units in the Yuanbaoshan region

The Yuanbaoshan region (our mapping area) is located in the southwestern section of the JO, where there is exposed Neoproterozic mélange, intruded granite and younger strata (Figs. 2, 3a). Near the Yuanbaoshan region, the mapped units include the Sibao Group, ca. 825 Ma Yuanbaoshan and Sangfang granitic plutons, the Danzhou Group, the Changan Formation, Cambrian–Ordovician strata and overlying Devonian–Carboniferous sediments (Fig. 3b) (BGMRGZ, 1965; BGMRGX, 1966; BGMRGX, 1967; BGMRGX, 1969). The Danzhou Group can be subdivided into the Baizhu, Hetong and Gongdong Formations from the base to top (Yang et al., 2015). Basic lithologies of the map units are briefly described below.

The Neoproterozoic metamorphic Sibao Group crops out under the Neoproterozoic–Cambrian sedimentary

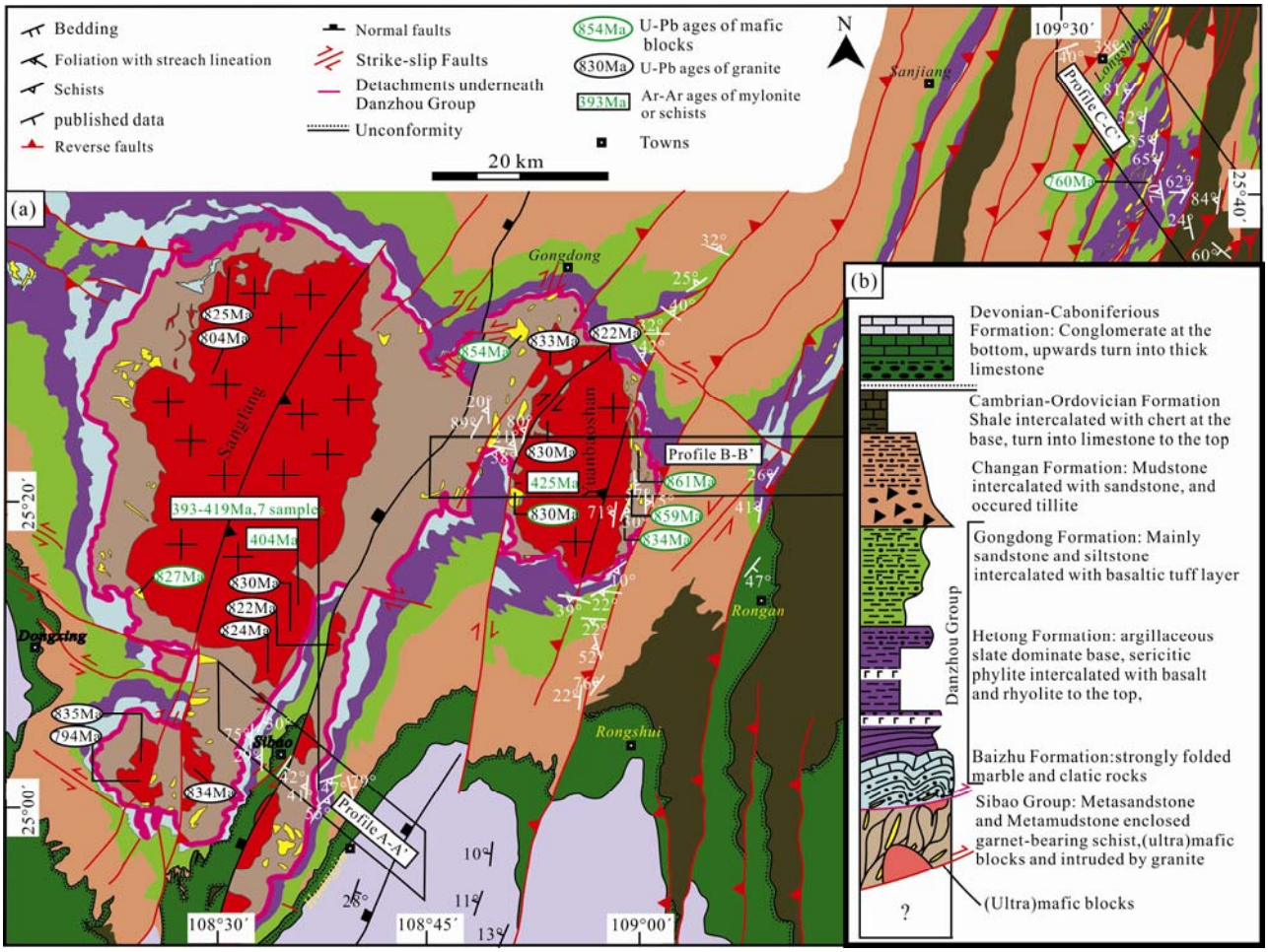


Fig. 3. Geological map and strata column.
(a), Simplified geological map of the Yuanbaoshan region in the northern Guangxi Province, south China. This geological map was based on 1:200,000 geological maps (BGMRGX, 1966; BGMRGX, 1967; BGMRGX, 1969; BGMRGZ, 1965). Different (thermo)geochronological results are cited from Chen et al., (2014); Li, (1999); Lin et al., (2015); Wang et al., (2013); Wang et al., (2014b); Wang et al., (2007); Yao et al., (2014); Zhang, (2015); Zhang Shitao et al., (2016c). The locations of 3D profiles in Figure 4 are in the black frame. (b), Stratigraphy of the mapping area, and the colors in the column coincide with Figure 3a and Figure 4.

rocks, and, in turn, is covered by the Devonian unconformity (Fig. 3a) (BGMRGX, 1967). From map view, the regional map pattern illustrates two north–south plunging dome structural patterns (Fig. 3a). The ca. 825 Ma Sangfang and Yuanbaoshan plutons, surrounded by the early Neoproterozoic mélange (Sibao Group), are present in the dome core. Lithologically, the Sibao Group includes interlayered metagraywacke, pelitic to mafic schists, quartzo–feldspathic gneiss, marble and garnet–bearing schist (BGMRGX, 1967; BGMRGX, 1969). It was intruded by undeformed Sangfang and Yuanbaoshang granites (Fig. 3a) (Yao et al., 2014c).

The unconformably–overlying Danzhou Group, composing the dome mantle, consists of strongly– to weakly–foliated terrestrial to marine sediments that are interbedded with several basaltic layers (Fig. 3b) (Ma et al., 2016). Stratigraphic successions surrounding the metamorphic rocks (Sibao Group and Danzhou Group) were divided into two units (Fig. 3b). The stratigraphically lowest unit is deformed shale and minor limestone that was assigned to the Changan and Cambrian–Ordovician Formations (Zhai, 2015). Unconformably overlying the deformed lower units are Devonian fossil–bearing sediments, which are capped by a Carboniferous limestone (Fig. 3b) (Chen et al., 2016).

We conducted structural mapping at three areas around the Yuanbaoshan pluton (based on 1:200,000 geological maps) (BGMRGZ, 1965; BGMRGX, 1966; BGMRGX, 1967; BGMRGX, 1969): near Sibao (Profile A–A'), Rongan (Profile B–B'), and in the Longsheng area (Profile C–C') (Fig. 3a). Based on stratigraphic comparisons, field data integration and map interpretation, we reconstructed three tectonic profiles from west to the east by using Move^{TM}.

3 Structural Geology

3.1 Western profile A–A'

The western profile A–A' is located on the southeastern flanks of the Sangfang pluton (Fig. 3a). The lowest Sibao Group, containing mafic rocks (Fig. 5a), are strongly deformed in profile A–A'. The bedding of the Sibao Group is occasionally observed and mainly strikes northwest–southeast and dips to the southwest, while the early foliations Ss_1 strike approximately north–south. The Ss_2 are dominantly dipping to the east at a high angle (Fig. 4a).

The unconformity between the underlying Sibao Group

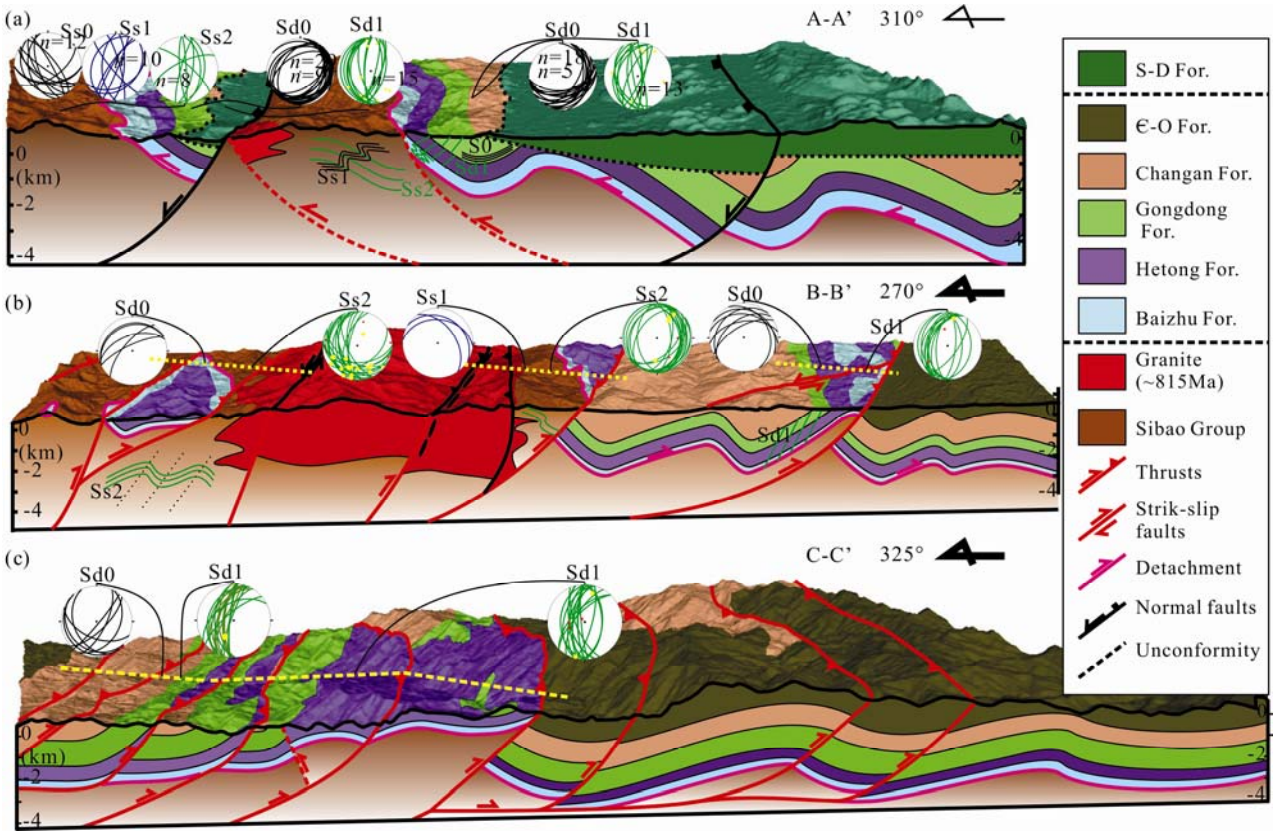


Fig. 4. Cross–sections (a) A–A', (b) B–B' and (c) C–C' located around the Yuanbaoshan region (detailed locations in Figure 3).
The 3D profiles were reconstructed using MoveTM (https://www.mve.com/). Tomography was downloaded from the USGS (https://earthexplorer.usgs.gov/) and masked by the geological map (Figure 3). During profile reconstruction, we attempted to maintain the thickness of the overlying sedimentary strata to fit outcrop exposures. The bedding attitudes of the strata are shown in the lower hemisphere, equal area projection stereonet plots.

and overlying Danzhou Group are documented in several published papers (Fig. 4a, line in pink) (Wang and Li, 2003; Yao et al., 2015a; Ma et al., 2016). The bedding of the Danzhou Group (Sd_0) mainly dips to the northwest or southeast, whereas the north–south–striking steep foliations (S_{d1}) are primarily dipping to the west at various dip angles (Fig. 4a). The Sd_1 is a pervasive axial cleavage (Fig. 5b–c) of the Danzhou Group, which is strongly

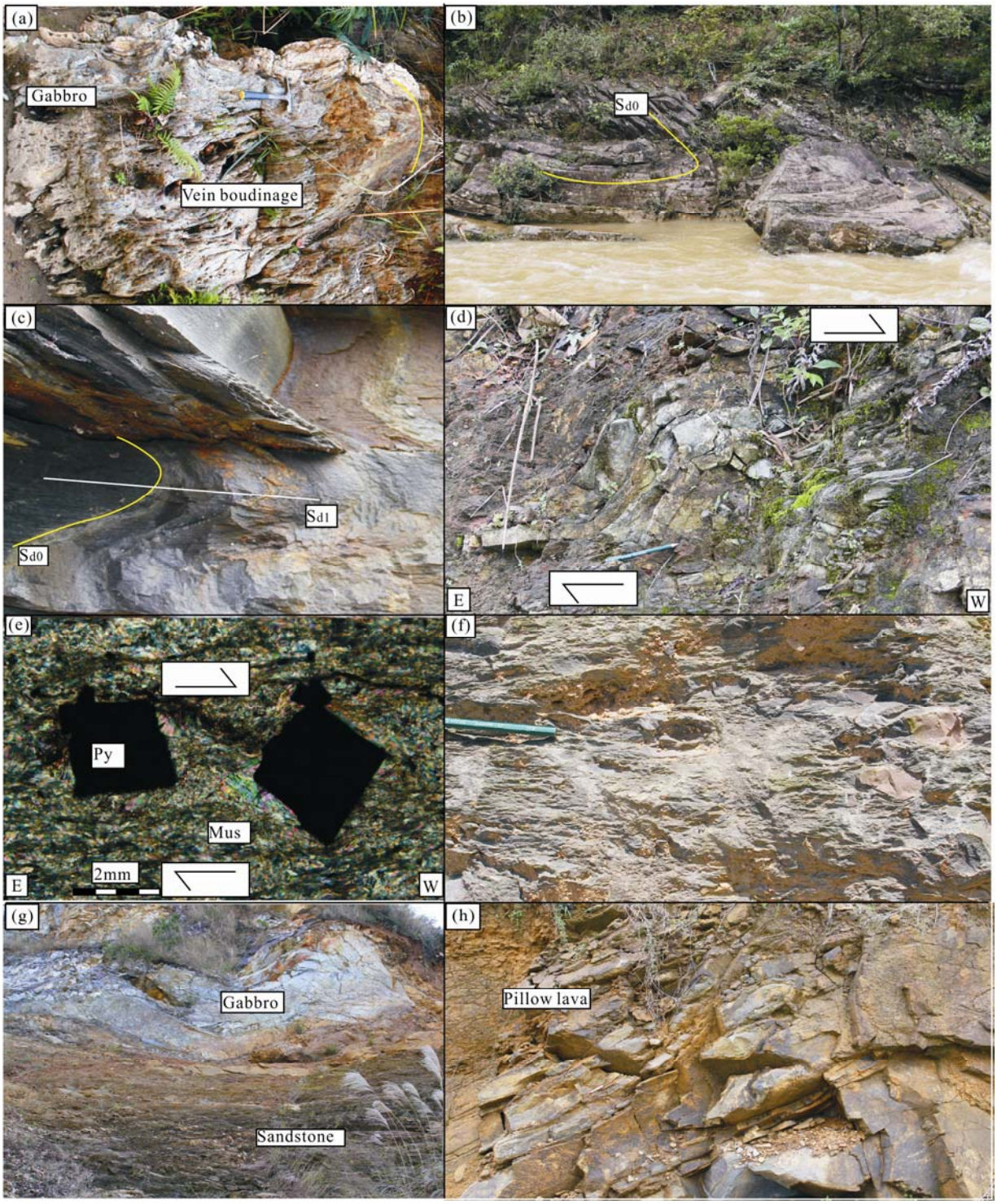


Fig. 5. Photographs illustrating the compositions and deformation in the profile.
(a), in the Sibao Group, a boudinage vein developed in a foliated gabbro. (b), tightly–folded Danzhou Group strata. (c), tightly–folded bedding Sd0 forming the axial cleavage Sd1 in the Danzhou Group. (d), a sandstone sigma porphyroblast indicates top–to–the–west shearing. (e), in thin section, pressure shadows of pyrite also show top–to–the–west movements. (f), diamictite in the Changan Formation does not show any deformation. (g), serpentinized gabbro blocks enclosed within deformed siltstone of the Sibao Group. (h), pillow lava within siltstone of the Sibao Group. (Abbreviation for all figures: Mus–muscovite, Py–pyrite, Grt–garnet, Qtz–quartz, Bi–biotite, Amp–amphibolite, Pl–plagioclase, Spl–spinel).

folded with north–south plunge hinges (Fig. 4a). Asymmetric folding and other shearing indicators, such as sigma porphyroblasts, indicate top–to–the–west shearing (Fig. 5d–e). We did not find older Sibao and Danzhou strata that were thrust westward onto the younger Phanerozoic strata (Fig. 4a, red dash line). However, it has been documented in areas farther west (Yan et al., 2003). The folded Danzhou Group is unconformably underlain by the undeformed Devonian limestone (Fig. 4a). Strong folding and S_{d1} only developed in the Danzhou Group but not in the overlying Devonian strata (Fig. 5f), which represents pre–Devonian tectonic events that are supported by white mica ^{40}Ar–^{39}Ar ages (section 5.3).

On the profile A–A', a normal fault (black line) separates the ~825 Ma granite from the Danzhou Group (Fig. 4a). This phase of normal faulting also cut through the overlying Devonian strata, so it must have occurred later than the Devonian, possibly during the Cretaceous (Li et al., 2016a).

3.2 Middle profile B–B'

The reconstructed middle profile B–B' (Fig. 4b) is located in the middle of mapping area and traverses the Yuanbaoshan pluton (Fig. 3a). The Sibao Group encloses (ultra)mafic blocks and pillow basalts (Fig. 5g–h) within the sedimentary mélange on western end of the profile B–B'. The bedding of the Sibao Group is hard to recognize in the field, however, an early phase of foliation in the Sibao Group (Ss_1) was observed both in the field (Fig. 6b) and in thin sections (Fig. 6c). The Ss_1 is mainly NW–SE striking. However, the cleavage Ss_2 mainly dips to the east at 10–30° on the eastern side of the Yuanbaoshan pluton, but dips to the west–southwest on the western side of the pluton (Fig. 4b). The deformed Sibao Group was intruded by undeformed Yuanbaoshan pluton (Fig. 6a) (Yao et al., 2014c). Near the undeformed Yuanbaoshan pluton, the Sibao Group illustrates top–to–the–east movements by asymmetric folds and sigma porphyroblasts, which indicate strong simple shear before the granitic intrusion (Fig. 6d–e). Thus, we interpret that these top–to–the–east shearing indicators formed in the subduction wedge during northwestward subduction of the Jiangnan oceanic lithosphere.

The Danzhou Group unconformably overlies the metamorphosed and deformed Sibao Group and granite (Fig. 4b). The base of the Danzhou Group (Baizhu and Hetong Formation) is located on both sides of the Yuanbaoshan pluton (Fig. 4b). After the granite intrusion, it must have experienced exhumation, otherwise the pluton cannot directly underlie the Danzhou Group (Ma et al., 2016). The Danzhou Group has northwest–northeast–dipping bedding Sd_0, whereas the newly formed axial cleavage Sd_1 by the folded Sd_0 is mainly dipping to the west at various dip angles (Fig. 4b). Both S_{s2} and Sd_1 strike north–south. Together, the north–south plunging fold hinges and east–west plunging stretching lineations indicate east–west shearing movements (Fig. 4b). We interpreted the subparallel Ss_2 and Sd_1 to have formed during the second phase of deformation that occurred after the deposition of the Danzhou Group.

The second phase of deformation is the dominant one in this region and was accompanied by coeval reverse faulting (Fig. 4b, red lines). In the center of the profile, two steeply westward–dipping mylonitic shear zones cut through the unfoliated granite (Fig. 6f), which show reverse movement and intensive stretching (Fig. 6f–g). Normally, reverse faults develop intensive quartz veins in the Danzhou Group, which indicates fluid activity during fault movement (Fig. 6h and Fig. 7a). Asymmetric folds, ductile reverse faults, kink bands, and S–C fabrics (Figs. 6h, 7a–b) within the faults indicate thrust faulting with an east–southeast displacement of the hanging wall relative to the footwall. The thrust became brittle and placed the Danzhou Group over the Cambrian limestone (Fig. 7c). Therefore, the fault movement could be younger than Cambrian. The mylonite exhibits westward plunging striations (Fig 4b, red dot). They are subparallel to the striations measured on the reverse fault surface, suggesting that the footwall mylonitic fabric is kinematically related to the thrust faulting. From the reconstructed profile B–B', we conclude that the thick–skinned thrust system exhumed the Sibao Group along several west–dipping thrusts, which repeated older rocks onto younger ones (Fig. 4b).

3.3 Eastern profile C–C'

The fold–thrust system dominates the eastern profile C–C' (Fig. 4c). Only the Danzhou Group, Changan Formation and Cambrian strata are exposed on this profile. The Danzhou Group is intercalated with several igneous layers and also intruded by mafic dikes (Fig. 7d). Far away from the reverse faults, the Danzhou Group is almost undeformed (Fig. 7e), but closer to the faults, tight recumbent faults developed (Fig. 7f), indicating coeval activity of the reverse faults and deformation of the Danzhou Group.

Almost all thrusts are northeast–striking and place the Danzhou group in the hanging wall over the Cambrian and Ordovician units in the footwall in the profile C–C' (Fig. 4c). The strata involved in the thrust fault exhibit a steep west–dipping foliation and westward–plunging stretching lineations that become progressively stronger toward the fault (Fig. 4c). A well–exposed example of a regional–scale thrust system crops out in the Longsheng area (Fig. 3a), an area teeming with talc mines that formed by fluid–

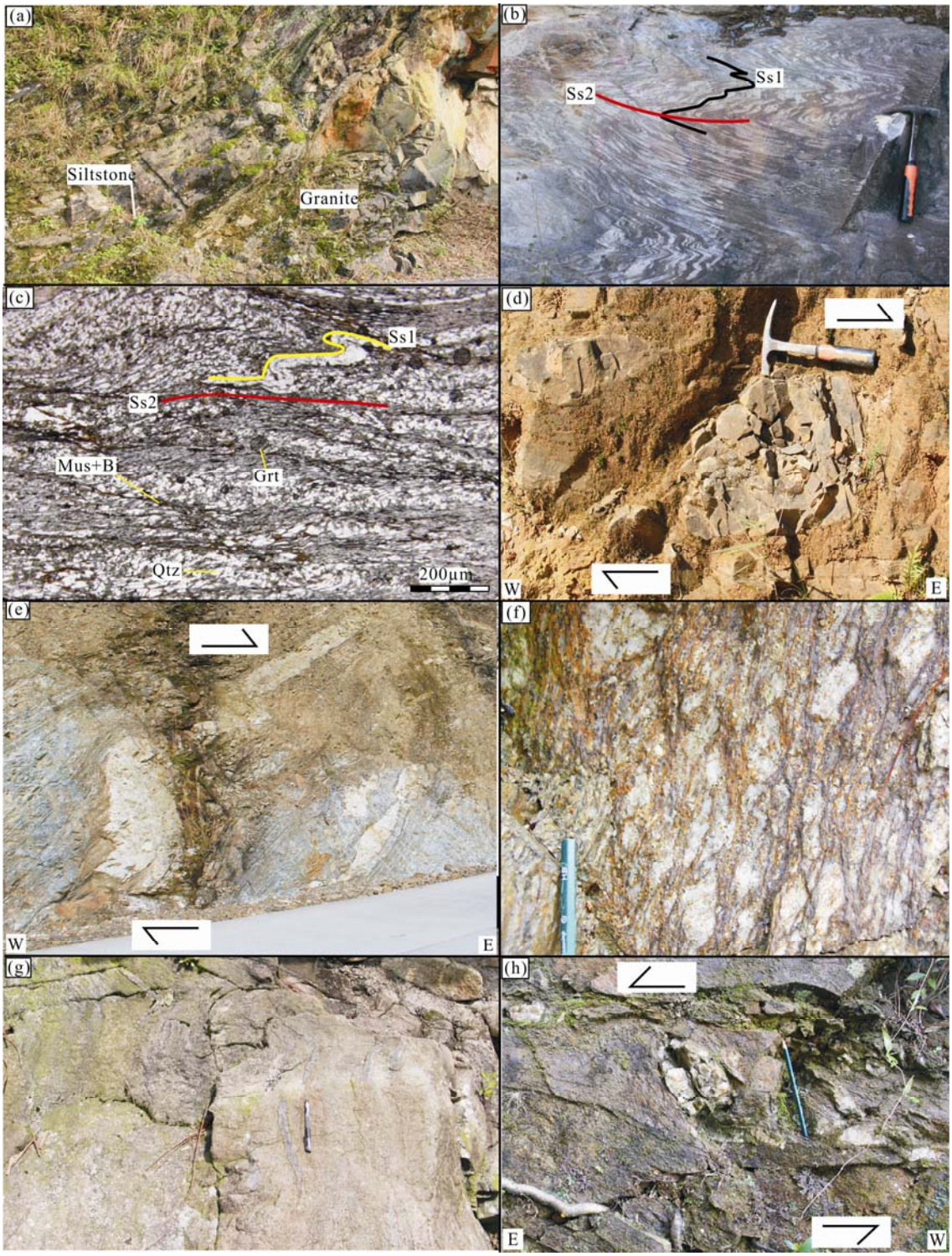


Fig. 6. Photographs illustrating the deformation of the Sibao Group in the section of the Yuanbaoshan region.
(a), undeformed Yuanbaoshan granite intruded the Sibao Group siltstone. (b), early phase foliation Ss1 refolded, forming new axial cleavage Ss2 on an outcrop of the Sibao Group. (c), in thin section, strongly–folded microlithon refolded and formed new cleavage Ss2, and during the second phase of deformation, garnet appeared. (d and e), west of the Yuanbaoshan pluton, the early phase of deformation is preserved. The sigma sharp sandstone in mudstone and large asymmetric quartz vein blocks indicated top–to–the–east displacements, which suggest westward subduction of the Jiangnan Ocean. (f), mylonitic granite west of the Yuanbaoshan pluton. (g), melanic enclaves were strongly stretched east of the Yuanbaoshan pluton. (h), a sigma quartz vein indicates top–to–the–east shearing in the Sibao Group.

rock interactions during thrust movement. The thrust faults have a top–to–the–east sense of tectonic transport (Fig. 7g), are widespread and affect all of the outcropping sedimentary units. The easternmost Cambrian units,

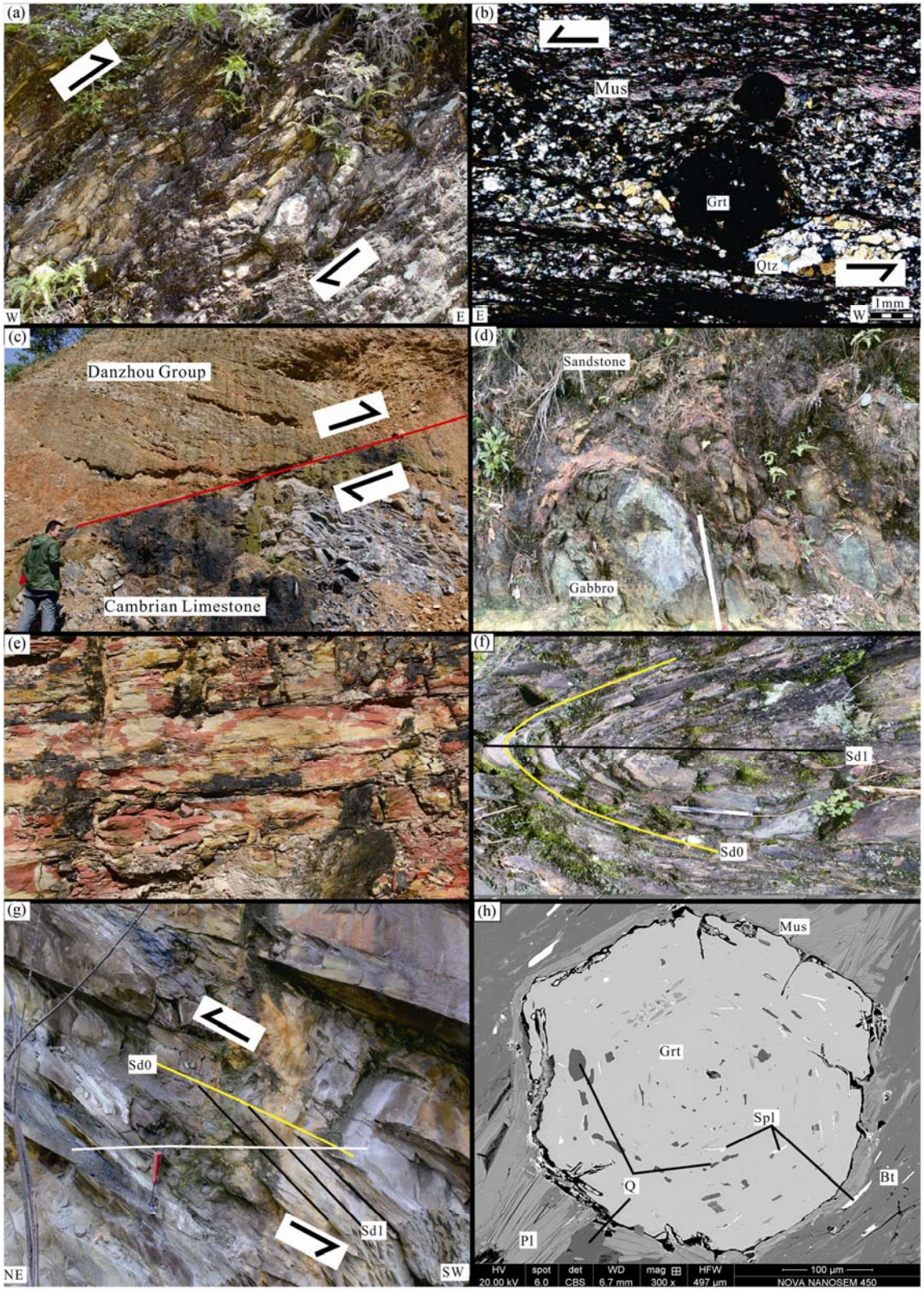


Fig. 7. Photographs illustrating the second phase of deformation in the B–B' section in the Yuanbaoshan region.

(a), the Danzhou Group is strongly foliated and fluid–saturated near the thrust fault, which also illustrate top–to–the–east shearing. (b), garnet–bearing mica schist records a general top–to–the–east movement, indicated by asymmetric quartz pressure shadows. Some muscovite grains are also oblique to the foliation. (c), the Danzhou Group thrust eastward onto the Cambrian limestone. (d), mafic blocks enclosed within a sandstone of the Danzhou Group. (e), undeformed Danzhou Group siltstone. (f), within the Danzhou Group, a recumbent fold overturned toward the east, with incipient flat–lying fracture cleavage in the Longsheng area. (g), sd1 clearly developed in the siltstone layer, combined with Sd0, shows top–to–the–northeast shearing. (h), garnet ring enclosing quartz, muscovite and spinel in the garnet–bearing schist of the Sibao Group, which records up to high –greenschist metamorphism.

located in the footwall, are internally deformed by north–south striking thrusts and gently southward–plunging folds (Fig. 4c).

3.4 Deformation phases

In the southwestern JO, there is lack of high–grade metamorphic rocks that prompted some authors to doubt the existence of an old in situ suture zone (e.g., Zhao et al., 2011). In our recent work, we found garnet–bearing mica schists in the eastern part of the Yuanbaoshan pluton (Fig. 7h) that may indicate high greenschist facies metamorphism (e.g., Gaidies et al., 2015). This indicates similar deformation and metamorphic conditions to the northeastern JO (Charvet et al., 2010). Moreover, the garnet formed pressure shadows parallel with the second phase of foliation, indicating the garnet formed before the second phase of D_2 deformation (Fig. 7c).

Based on above description, we concluded that D_1 deformation, which only occurred in the Sibao Group, lead to the Ss_1 schistosity develop in the Sibao Group. The D_2 deformation must younger than deposition of the Danzhou Group, which expresses as Ss_2 and Sd_1 in the Sibao and Danzhou Group, respectively. During the first deformation D_1, the Sibao Group probably experience high greenschist facies metamorphism due to deep burial or contact metamorphism by Yuanbaoshan pluton intrusion.

Coeval with D_2, the fault systems in Yuanbaoshan and around the region bound two domains. From the Yuanbaoshan pluton in the east, the pre–Devonian metamorphic units show a ductile to brittle deformation with an eastward vergence expressed in a more ductile manner towards the base of the Danzhou Group. To the west of the Yuanbaoshan pluton, the vergence is towards the west, and widely documented as a thin–skinned thrust system (Yan et al., 2003). These results suggest a positive flower structure and agree with the documented tectonic findings in the northeast Jiangnan Orogen by Charvet et al. (2010). Several locations of main thrusts show that there could be a décollement underneath the Danzhou Group, which grades structurally downward into mylonitic schists and gneisses. It may flatten at depth, according to the reconstructed profile (Fig. 4b–c, line in pink). This interpretation could also reasonably explain the abundant fluid provenance and activity.

4 Geochronology

In this study, we present (detrital) zircon U–Pb results and white mica $^{40}Ar/^{39}Ar$ ages that in conjunction with the structural geology, providing additional constraints on the tectonics of the southwestern JO. U–Pb zircon geochronology was used (1) to constrain the maximum depositional age of stratigraphic horizons using the youngest distinct age group (Dickinson and Gehrels, 2009) and (2) to determine the provenance of the sampled strata (Cawood et al., 2012). Moreover, white mica $^{40}Ar/^{39}Ar$ ages were used to constrain the latest cooling event in the Yuanbaoshan region.

4.1 Sampling and methods

Zircons were separated using standard mineral separation techniques, mounted in epoxy with fragments, and polished to a depth of ca. 20 μm. Then, a series of back–scattered images (BSE) were produced using a Scanning Electron Microscope (SEM). The cores of zircons were then analyzed by a laser ablation multi collector inductively coupled plasma mass spectrometer (LA–ICP–MS) at the China University of Geosciences. Zircons were selected at random and a minimum of 60 grains per sample was analyzed. Details of the U–Pb analytical method have been described by Liu et al. (2010). Uncertainties on individual analyses in the data table and concordia plots are presented at 1σ, whereas errors on averages of multiple analyses are given at the 2σ level. Analyses that show greater than 10% discordance were not included in the frequency diagrams. Ages less than 1000 Ma are based on the $^{206}Pb/^{238}U$ ratio, whereas older ages are based on the $^{207}Pb/^{206}Pb$ ratio. Detrital U–Pb dating results are presented as relative probability diagrams (Fig. 8); tabulated results are available in the (Table 1).

In total, eight samples were dated. Sample 041003–D, 040906–D1 and 120904–D1 are metasandstones and sampled from the Sibao Group. Sample 041805–D1 is derived from the Danzhou Group near the Longsheng area (Fig. 3a). Sample 040704–D1 was sampled from the Changan Group and the Cambrian conglomerate 040703–D1 was dated as well. The Yuanbaoshan granite (041001–D1) and a basaltic tuff layer within the Danzhou Group, Sample (040808–D1), were also dated. The average of the younger ages from the granite (041001–D1) and basaltic tuff (040808–D1) are plotted, too (Fig. 8).

The $^{40}Ar/^{39}Ar$ dating was performed at the Laboratory of Isotope Thermochronology (LIF), Institute of Geology, Chinese Academy of Geological Sciences (CAGS) (Beijing, China). The samples were ultrasonically cleaned, wrapped in aluminum foil and loaded into aluminum tubes, together with 2 or 3 monitor samples (ZBH–25). See Yin et al. (2015) for a detailed description of the procedure. The uncertainty of each apparent age is one standard deviation. The monitor (ZBH–25), used as an internal standard, is Fangshan biotite with an age of 132.7±1.2 Ma and potassium (K) content of 7.579±0.030 wt% (Wang Sungshan, 1983). The $^{40}Ar/^{39}Ar$ dating results

Table 1 Individual spot measurements for the zircon geochronology

Analysis	Corrected ratios					Corrected ages (Ma)				Concordance limit
	$^{207}Pb/^{206}Pb$	± 1σ	$^{206}Pb/^{238}U$	± 1σ	rho	$^{207}Pb/^{206}Pb$	± 1σ	$^{206}Pb/^{238}U$	± 1σ	
Sample 040703-D1: Cambrian conglomerate GPS: N25°06'07'', E109°11'29''										
0703-Z1-01	2.40	0.11	0.20	0.00	0.41	1322.22	80.56	1196.20	20.17	0.96
0703-Z1-02	1.75	0.06	0.15	0.00	0.33	1277.78	70.37	903.43	9.91	87%
0703-Z1-03	8.51	0.27	0.42	0.01	0.38	2279.63	53.25	2269.28	23.34	99%
0703-Z1-04	11.88	0.33	0.49	0.01	0.42	2598.15	45.99	2569.49	24.57	99%
0703-Z1-05	1.78	0.06	0.17	0.00	0.44	1084.88	84.11	1022.44	14.90	98%
0703-Z1-06	1.82	0.05	0.18	0.00	0.34	1053.71	51.85	1042.45	8.29	99%
0703-Z1-07	11.67	0.34	0.49	0.01	0.44	2590.43	50.00	2558.69	26.95	99%
0703-Z1-08	2.20	0.05	0.20	0.00	0.36	1175.93	52.77	1173.16	9.30	99%
0703-Z1-09	1.72	0.10	0.17	0.00	0.42	1038.90	114.82	1025.65	23.79	99%
0703-Z1-10	14.76	0.23	0.54	0.00	0.48	2793.52	26.39	2798.78	17.42	99%
0703-Z1-11	1.64	0.03	0.17	0.00	0.44	964.81	43.52	992.29	8.08	99%
0703-Z1-12	1.69	0.05	0.17	0.00	0.48	990.74	27.78	1009.94	12.44	99%
0703-Z1-13	1.45	0.04	0.15	0.00	0.56	809.26	64.81	920.93	13.80	98%
0703-Z1-14	1.82	0.06	0.18	0.00	0.38	1050.01	69.44	1053.66	12.67	99%
0703-Z1-15	3.04	0.07	0.25	0.00	0.44	1375.93	43.37	1440.52	12.89	98%
0703-Z1-16	1.47	0.04	0.15	0.00	0.41	924.07	47.69	911.17	8.84	99%
0703-Z1-17	3.55	0.08	0.27	0.00	0.44	1555.25	44.75	1519.52	13.99	98%
0703-Z1-18	2.10	0.06	0.19	0.00	0.52	1147.23	51.85	1142.59	15.03	99%
0703-Z1-19	10.40	0.26	0.46	0.01	0.49	2468.20	36.88	2455.66	24.90	99%
0703-Z1-20	1.84	0.05	0.18	0.00	0.47	1055.56	59.26	1064.81	13.43	99%
0703-Z1-21	1.37	0.03	0.15	0.00	0.52	861.11	40.74	875.84	8.70	99%
0703-Z1-22	4.23	0.09	0.30	0.00	0.44	1677.78	40.74	1674.44	14.27	99%
0703-Z1-23	0.95	0.06	0.11	0.00	0.32	701.86	156.46	682.81	13.98	99%
0703-Z1-24	4.16	0.12	0.30	0.00	0.47	1642.59	53.55	1676.39	19.90	99%
0703-Z1-25	1.98	0.05	0.19	0.00	0.56	1084.88	48.92	1109.63	13.86	99%
0703-Z1-26	7.91	0.24	0.40	0.01	0.46	2242.60	54.17	2184.21	25.93	98%
0703-Z1-27	0.93	0.03	0.11	0.00	0.35	675.94	66.66	653.78	6.31	98%
0703-Z1-28	0.78	0.02	0.10	0.00	0.44	553.74	68.51	587.72	7.34	99%
0703-Z1-29	1.62	0.04	0.16	0.00	0.39	1000.00	60.34	977.30	9.43	99%
0703-Z1-30	11.44	0.33	0.49	0.01	0.62	2505.56	45.37	2576.49	38.29	99%
0703-Z1-31	1.81	0.04	0.18	0.00	0.46	1009.26	93.52	1047.28	10.36	99%
0703-Z1-32	10.48	0.25	0.45	0.01	0.48	2510.19	52.63	2386.86	22.39	96%
0703-Z1-33	14.80	0.42	0.56	0.01	0.57	2708.95	55.55	2876.64	37.95	97%
0703-Z1-34	10.21	0.29	0.46	0.01	0.53	2421.91	54.93	2450.47	30.60	99%
0703-Z1-35	1.45	0.04	0.15	0.00	0.50	864.81	64.81	914.64	12.71	99%
0703-Z1-36	10.91	0.26	0.48	0.01	0.48	2472.53	44.44	2534.10	24.51	99%
0703-Z1-37	16.36	0.48	0.57	0.01	0.42	2860.80	43.98	2909.89	28.43	99%
0703-Z1-38	11.88	0.33	0.49	0.01	0.43	2594.45	44.45	2571.35	25.59	99%
0703-Z1-39	1.75	0.06	0.18	0.00	0.38	964.81	62.96	1046.51	12.40	98%
0703-Z1-40	1.05	0.04	0.12	0.00	0.28	727.79	77.77	722.52	7.17	99%
0703-Z1-41	1.24	0.05	0.14	0.00	0.36	881.17	311.10	818.22	11.93	99%
0703-Z1-42	3.66	0.12	0.28	0.00	0.35	1542.60	55.87	1569.85	16.25	99%
0703-Z1-43	3.22	0.11	0.26	0.00	0.36	1428.70	56.02	1472.40	15.83	99%
0703-Z1-44	11.24	0.27	0.48	0.00	0.38	2542.90	37.35	2526.46	19.32	99%
0703-Z1-45	1.27	0.04	0.14	0.00	0.43	810.80	54.78	836.28	9.37	99%
0703-Z1-46	0.77	0.02	0.09	0.00	0.42	572.26	62.95	580.45	6.54	99%
0703-Z1-47	11.16	0.21	0.48	0.00	0.45	2600.00	32.25	2520.60	17.68	99%
0703-Z1-48	2.95	0.07	0.24	0.00	0.44	1387.04	47.07	1388.39	12.91	99%
0703-Z1-49	1.38	0.06	0.15	0.00	0.36	875.93	87.04	875.60	12.29	99%
0703-Z1-50	3.02	0.09	0.24	0.00	0.51	1416.97	44.91	1398.58	18.51	98%
0703-Z1-51	1.39	0.03	0.15	0.00	0.51	862.65	45.22	885.32	10.20	99%
0703-Z1-52	1.71	0.03	0.17	0.00	0.40	961.11	46.45	1029.96	7.83	98%
0703-Z1-53	10.62	0.22	0.47	0.01	0.53	2484.26	30.56	2487.97	22.44	99%
0703-Z1-54	0.87	0.03	0.10	0.00	0.34	655.57	66.66	629.74	6.47	99%
0703-Z1-55	1.90	0.08	0.18	0.00	0.37	1081.17	79.63	1079.82	14.82	99%
0703-Z1-56	1.43	0.07	0.15	0.00	0.36	1000.00	98.15	898.88	13.95	99%
Sample 040704-D1: Changan Formation sandstone GPS: N25°07'52'', E109°11'53''										
0704-Z1-01	6.59	0.13	0.38	0.00	0.47	2027.47	37.19	2092.01	17.06	98%
0704-Z1-02	11.01	0.22	0.46	0.00	0.50	2599.69	29.94	2423.30	20.20	95%
0704-Z1-03	1.12	0.03	0.12	0.00	0.36	781.17	55.55	759.09	7.07	99%
0704-Z1-04	1.38	0.02	0.14	0.00	0.40	953.70	35.19	852.94	5.70	96%
0704-Z1-05	6.05	0.12	0.36	0.00	0.46	2003.39	35.18	1966.86	15.53	99%
0704-Z1-06	11.05	0.16	0.48	0.00	0.54	2527.47	22.38	2522.07	16.95	99%
0704-Z1-07	13.02	0.19	0.51	0.00	0.58	2692.28	20.37	2661.61	18.30	99%
0704-Z1-08	7.71	0.13	0.37	0.00	0.54	2358.34	33.02	2032.24	16.44	92%
0704-Z1-09	1.27	0.04	0.14	0.00	0.40	842.59	76.85	835.60	10.54	99%
0704-Z1-10	10.63	0.19	0.45	0.00	0.46	2587.04	27.47	2373.62	16.08	95%
0704-Z1-11	9.76	0.19	0.43	0.00	0.56	2483.02	26.09	2321.10	21.68	96%

Continued Table 1

Analysis	Corrected ratios					Corrected ages (Ma)				Concordance limit
	$^{207}Pb/^{206}Pb$		$^{206}Pb/^{238}U$			$^{207}Pb/^{206}Pb$		$^{206}Pb/^{238}U$		
	± 1σ		± 1σ		rho	± 1σ		± 1σ		
0704-Z1-12	1.22	0.04	0.14	0.00	0.36	1200.00	60.95	817.22	8.51	99%
0704-Z1-13	1.59	0.04	0.15	0.00	0.40	1131.49	50.31	893.79	8.55	92%
0704-Z1-14	1.18	0.03	0.13	0.00	0.40	775.93	50.77	798.43	6.99	99%
0704-Z1-15	1.19	0.03	0.13	0.00	0.42	816.67	58.33	791.01	7.68	99%
0704-Z1-16	6.46	0.15	0.38	0.00	0.43	1992.28	41.05	2079.76	18.28	98%
0704-Z1-17	1.43	0.04	0.15	0.00	0.41	898.15	55.56	899.19	8.89	99%
0704-Z1-18	1.39	0.04	0.15	0.00	0.45	864.81	137.20	892.29	11.04	99%
0704-Z1-19	6.61	0.15	0.38	0.00	0.52	2055.55	39.66	2064.54	21.36	99%
0704-Z1-20	1.24	0.04	0.14	0.00	0.41	725.62	68.51	852.30	9.46	96%
0704-Z1-21	1.32	0.04	0.14	0.00	0.46	810.80	55.55	870.48	10.50	98%
0704-Z1-22	1.12	0.05	0.13	0.00	0.45	861.11	159.25	776.95	15.07	98%
0704-Z1-23	1.08	0.03	0.13	0.00	0.42	655.57	66.66	780.07	9.71	95%
0704-Z1-24	1.00	0.03	0.12	0.00	0.33	675.94	49.07	708.50	5.69	99%
0704-Z1-25	5.29	0.11	0.33	0.00	0.47	1933.34	34.56	1860.64	15.92	99%
0704-Z1-26	9.08	0.20	0.44	0.01	0.58	2333.03	31.33	2358.68	24.81	99%
0704-Z1-27	1.21	0.04	0.13	0.00	0.38	835.18	66.67	800.16	9.13	99%
0704-Z1-28	5.38	0.15	0.33	0.00	0.48	1918.21	46.30	1851.12	20.92	98%
0704-Z1-29	1.17	0.03	0.14	0.00	0.43	683.35	50.00	824.43	8.18	95%
0704-Z1-30	7.75	0.13	0.39	0.00	0.43	2271.92	27.47	2123.03	12.96	96%
0704-Z1-31	1.21	0.03	0.14	0.00	0.43	753.71	51.85	824.90	8.58	97%
0704-Z1-32	9.58	0.16	0.45	0.00	0.57	2388.58	24.53	2394.59	19.33	99%
0704-Z1-33	4.44	0.14	0.30	0.00	0.51	1753.70	54.17	1701.51	23.01	98%
0704-Z1-34	1.16	0.03	0.13	0.00	0.41	790.74	50.77	777.75	7.19	99%
0704-Z1-35	1.43	0.03	0.15	0.00	0.38	924.07	43.36	888.56	7.04	98%
0704-Z1-36	5.92	0.14	0.35	0.00	0.44	1984.26	44.60	1945.51	16.93	99%
0704-Z1-37	1.01	0.05	0.11	0.00	0.30	687.05	99.06	659.02	8.87	92%
0704-Z1-38	5.74	0.14	0.35	0.00	0.39	1944.14	35.34	1928.92	16.10	99%
0704-Z1-39	1.19	0.04	0.13	0.00	0.30	787.04	67.43	803.83	8.09	99%
0704-Z1-40	1.28	0.07	0.14	0.00	0.30	857.40	113.89	843.74	13.92	99%
0704-Z1-41	10.20	0.40	0.47	0.01	0.28	2442.28	51.85	2466.40	22.29	99%
0704-Z1-42	1.06	0.05	0.12	0.00	0.25	731.49	77.62	736.16	8.42	99%
0704-Z1-43	1.16	0.09	0.13	0.00	0.23	783.34	188.41	813.77	13.61	96%
0704-Z1-44	9.61	0.38	0.45	0.01	0.29	2399.08	55.86	2399.94	23.13	99%
0704-Z1-45	1.41	0.07	0.15	0.00	0.38	927.78	114.05	896.08	16.28	99%
0704-Z1-46	1.12	0.05	0.13	0.00	0.27	731.49	77.62	778.85	7.96	98%
0704-Z1-47	3.96	0.10	0.28	0.00	0.36	1631.48	42.12	1616.33	13.26	99%
0704-Z1-48	1.46	0.05	0.15	0.00	0.29	894.45	67.59	915.83	7.97	99%
0704-Z1-49	9.84	0.25	0.46	0.01	0.51	2413.27	43.98	2434.71	26.26	99%
0704-Z1-50	1.08	0.03	0.12	0.00	0.49	750.01	47.07	737.17	8.00	99%
0704-Z1-51	1.08	0.03	0.12	0.00	0.45	661.13	72.21	743.19	8.89	99%
0704-Z1-52	1.49	0.08	0.16	0.00	0.38	1061.12	174.84	937.02	17.06	98%
0704-Z1-53	5.31	0.10	0.34	0.00	0.54	1855.56	32.10	1885.20	16.73	99%
0704-Z1-54	9.99	0.18	0.46	0.00	0.55	2409.26	27.77	2455.63	19.91	99%
0704-Z1-55	10.61	0.19	0.48	0.01	0.59	2472.22	27.16	2506.74	22.64	99%
0704-Z1-56	9.37	0.16	0.45	0.00	0.53	2371.92	27.47	2374.74	18.32	99%
0704-Z1-57	1.39	0.07	0.15	0.00	0.45	883.33	111.11	900.77	18.20	98%
0704-Z1-58	1.44	0.04	0.15	0.00	0.36	966.67	61.11	881.42	8.82	97%
0704-Z1-59	1.11	0.04	0.13	0.00	0.57	724.08	91.66	765.26	14.94	99%
0704-Z1-60	1.22	0.09	0.13	0.01	0.58	972.23	164.82	802.67	31.06	99%
0704-Z1-61	12.58	0.24	0.50	0.00	0.44	2661.12	29.63	2623.83	18.40	99%
0704-Z1-62	6.82	0.24	0.38	0.01	0.44	2087.96	58.80	2088.06	28.05	99%
0704-Z1-63	1.49	0.05	0.15	0.00	0.29	970.06	66.67	905.65	7.85	97%
0704-Z1-64	1.20	0.08	0.13	0.00	0.34	766.67	146.29	793.51	17.78	99%
0704-Z1-65	12.37	0.43	0.50	0.01	0.46	2653.71	60.96	2610.42	34.69	99%
Sample 041805-D1: Sandstone			**GPS: N25°36'42'', E109°49'16''**							
1805-Z1-01	1.98	0.11	0.11	0.00	0.25	2105.86	94.60	669.91	8.79	50%
1805-Z1-02	1.35	0.05	0.14	0.00	0.31	966.67	77.78	838.16	8.89	96%
1805-Z1-03	10.34	0.15	0.46	0.00	0.56	2475.61	22.07	2445.87	16.82	99%
1805-Z1-04	5.75	0.12	0.35	0.00	0.56	1944.14	26.85	1926.69	18.92	99%
1805-Z1-05	2.89	0.05	0.24	0.00	0.57	1384.26	29.63	1373.43	11.74	99%
1805-Z1-06	1.43	0.06	0.14	0.00	0.37	1125.00	93.98	826.01	12.81	91%
1805-Z1-07	1.24	0.05	0.14	0.00	0.33	768.52	85.18	837.40	10.56	97%
1805-Z1-08	5.62	0.12	0.33	0.00	0.43	1972.53	36.73	1861.55	15.26	96%
1805-Z1-09	6.28	0.18	0.35	0.00	0.45	2097.84	47.22	1940.12	21.85	96%
1805-Z1-10	1.36	0.03	0.14	0.00	0.44	938.89	43.67	841.99	7.11	96%
1805-Z1-11	10.14	0.16	0.46	0.00	0.63	2458.94	24.38	2423.53	20.67	98%
1805-Z1-12	1.29	0.03	0.14	0.00	0.38	873.76	45.37	826.69	7.20	98%
1805-Z1-13	5.91	0.20	0.30	0.00	0.42	2287.04	70.68	1689.99	20.59	85%
1805-Z1-14	2.16	0.10	0.13	0.00	0.26	1931.49	77.01	796.45	9.23	62%

Continued Table 1

Analysis	Corrected ratios					Corrected ages (Ma)				Concordance limit
	$^{207}Pb/^{206}Pb$		$^{206}Pb/^{238}U$		rho	$^{207}Pb/^{206}Pb$		$^{206}Pb/^{238}U$		
	± 1σ		± 1σ			± 1σ		± 1σ		
1805-Z1-15	1.34	0.05	0.14	0.00	0.39	942.59	77.01	839.32	10.63	97%
1805-Z1-16	1.23	0.03	0.13	0.00	0.42	809.26	55.55	813.98	8.21	99%
1805-Z1-17	1.17	0.03	0.13	0.00	0.39	809.26	63.89	775.14	7.74	98%
1805-Z1-18	4.43	0.08	0.30	0.00	0.46	1727.78	31.63	1701.56	11.91	99%
1805-Z1-19	9.90	0.16	0.45	0.00	0.56	2435.49	26.69	2405.23	17.76	99%
1805-Z1-20	9.33	0.14	0.43	0.00	0.47	2427.78	24.38	2294.09	13.85	96%
1805-Z1-21	6.15	0.09	0.32	0.00	0.46	2186.73	24.69	1809.02	10.66	90%
1805-Z1-22	12.41	0.24	0.49	0.00	0.50	2679.63	27.78	2568.31	20.01	97%
1805-Z1-23	1.43	0.04	0.15	0.00	0.36	875.93	47.22	909.53	7.56	99%
1805-Z1-24	1.62	0.08	0.15	0.00	0.31	1194.45	105.71	882.94	13.01	89%
1805-Z1-25	1.35	0.06	0.14	0.00	0.34	987.04	87.96	824.58	11.76	95%
1805-Z1-26	10.73	0.18	0.47	0.00	0.53	2503.39	26.55	2489.41	18.25	99%
1805-Z1-27	1.38	0.05	0.15	0.00	0.26	872.22	128.71	885.34	7.22	99%
1805-Z1-28	6.37	0.12	0.37	0.00	0.47	2038.89	34.72	2020.29	14.97	99%
1805-Z1-29	3.17	0.08	0.25	0.00	0.46	1442.60	44.44	1454.50	14.35	99%
1805-Z1-30	10.26	0.63	0.41	0.01	0.29	2592.28	71.15	2200.58	32.89	88%
1805-Z1-31	10.84	0.24	0.43	0.00	0.43	2700.00	34.72	2289.06	18.30	90%
1805-Z1-32	1.51	0.05	0.16	0.00	0.29	855.55	66.67	971.89	9.15	96%
1805-Z1-33	1.54	0.10	0.15	0.00	0.46	1110.80	151.54	886.21	24.24	93%
1805-Z1-34	10.51	0.18	0.45	0.00	0.54	2536.72	25.62	2408.64	18.26	97%
1805-Z1-35	1.22	0.03	0.13	0.00	0.33	812.96	48.14	809.38	5.68	99%
1805-Z1-36	12.13	0.20	0.49	0.00	0.57	2627.78	19.91	2591.38	20.46	99%
1805-Z1-37	1.12	0.03	0.13	0.00	0.42	742.60	48.14	765.29	7.14	99%
1805-Z1-38	1.34	0.03	0.14	0.00	0.47	850.00	45.37	864.55	7.43	99%
1805-Z1-39	7.18	0.16	0.39	0.00	0.47	2142.28	39.20	2119.73	18.45	99%
1805-Z1-40	11.21	0.20	0.48	0.00	0.56	2531.79	29.01	2536.37	21.00	99%
1805-Z1-41	3.47	0.22	0.15	0.00	0.37	2439.20	83.79	924.80	20.62	51%
1805-Z1-42	10.60	0.19	0.45	0.00	0.61	2561.42	29.32	2389.26	22.11	95%
1805-Z1-43	1.27	0.04	0.14	0.00	0.37	833.33	73.15	830.00	9.93	99%
1805-Z1-44	6.70	0.11	0.38	0.00	0.55	2055.55	27.77	2088.41	16.28	99%
1805-Z1-45	9.46	0.17	0.43	0.01	0.67	2442.59	30.55	2303.51	23.65	96%
1805-Z1-46	7.62	0.15	0.40	0.00	0.42	2202.16	32.57	2157.68	15.13	98%
1805-Z1-47	1.32	0.04	0.14	0.00	0.43	835.18	55.56	858.58	9.34	99%
1805-Z1-48	1.48	0.05	0.15	0.00	0.37	1016.67	63.43	877.33	9.86	95%
1805-Z1-49	5.43	0.12	0.32	0.00	0.47	1998.15	37.03	1785.21	15.76	94%
1805-Z1-50	5.61	0.15	0.28	0.00	0.39	2299.69	42.60	1575.72	14.75	80%
1805-Z1-51	1.37	0.06	0.14	0.00	0.34	1009.26	81.95	819.58	11.33	93%
1805-Z1-52	2.65	0.12	0.14	0.00	0.30	2173.15	72.53	843.72	10.53	56%
1805-Z1-53	11.49	0.40	0.42	0.01	0.46	2794.14	42.28	2245.45	30.09	86%
1805-Z1-54	1.36	0.04	0.14	0.00	0.46	875.93	128.71	867.80	11.47	99%
1805-Z1-55	1.32	0.04	0.14	0.00	0.35	827.78	58.18	861.63	7.61	99%
1805-Z1-56	10.90	0.22	0.47	0.00	0.43	2525.61	33.95	2489.85	18.04	99%
1805-Z1-57	1.85	0.05	0.17	0.00	0.38	1188.58	55.09	1005.05	9.59	94%
1805-Z1-58	2.00	0.08	0.14	0.00	0.22	1701.85	81.94	845.09	7.38	72%
1805-Z1-59	1.29	0.06	0.14	0.00	0.31	853.70	90.74	837.49	10.71	99%
1805-Z1-60	1.40	0.04	0.14	0.00	0.32	1017.59	56.02	838.94	6.92	94%
1805-Z1-61	1.33	0.05	0.13	0.00	0.29	966.67	66.67	814.30	8.11	94%
1805-Z1-62	1.23	0.04	0.13	0.00	0.33	835.18	63.43	805.99	7.45	99%
1805-Z1-63	1.26	0.04	0.14	0.00	0.37	857.40	67.75	822.85	8.81	99%
1805-Z1-64	1.31	0.03	0.14	0.00	0.43	872.22	41.67	840.89	8.06	99%
1805-Z1-65	1.38	0.04	0.15	0.00	0.36	879.63	59.26	877.03	9.12	99%
Sample 040906-D1: Metasandstone			**GPS: N25°19'55", E109°15'34"**							
0906-Z1-01	1.51	0.03	0.16	0.00	0.39	864.81	36.11	963.87	6.84	97%
0906-Z1-02	12.88	0.24	0.52	0.01	0.70	2653.40	22.38	2679.00	28.79	99%
0906-Z1-03	1.55	0.04	0.16	0.00	0.48	1000.00	50.00	953.16	11.12	99%
0906-Z1-04	10.66	0.18	0.48	0.00	0.56	2449.07	21.30	2542.41	20.01	98%
0906-Z1-05	1.82	0.05	0.18	0.00	0.44	1025.61	56.02	1071.05	11.85	98%
0906-Z1-06	5.26	0.07	0.34	0.00	0.56	1805.56	24.07	1910.23	12.80	97%
0906-Z1-07	1.48	0.03	0.16	0.00	0.39	872.22	37.04	940.79	6.54	98%
0906-Z1-08	14.45	0.25	0.55	0.01	0.65	2746.30	23.30	2817.90	25.72	98%
0906-Z1-09	10.90	0.18	0.48	0.01	0.67	2484.87	22.22	2542.49	22.83	98%
0906-Z1-10	1.43	0.02	0.15	0.00	0.57	835.18	28.86	923.43	7.22	97%
0906-Z1-11	10.53	0.16	0.48	0.00	0.69	2446.60	19.29	2516.06	21.22	98%
0906-Z1-12	15.62	0.20	0.47	0.00	0.60	3131.49	12.81	2471.05	15.89	85%
0906-Z1-13	8.17	0.11	0.41	0.00	0.71	2262.66	20.37	2229.50	17.97	99%
0906-Z1-14	15.52	0.20	0.58	0.00	0.52	2761.12	20.68	2961.90	15.83	96%
0906-Z1-15	5.46	0.13	0.34	0.00	0.45	1933.34	35.65	1908.88	17.18	99%
0906-Z1-16	14.00	0.22	0.53	0.00	0.58	2733.03	23.92	2761.28	20.66	99%
0906-Z1-17	1.69	0.04	0.17	0.00	0.49	999.08	36.89	1005.04	9.59	99%

Continued Table 1

Analysis	Corrected ratios					Corrected ages (Ma)				Concordance limit
	$^{207}Pb/^{206}Pb$		$^{206}Pb/^{238}U$			$^{207}Pb/^{206}Pb$		$^{206}Pb/^{238}U$		
	± 1σ		± 1σ		rho	± 1σ		± 1σ		
0906-Z1-18	4.92	0.08	0.32	0.00	0.63	1809.26	27.47	1794.11	16.75	99%
0906-Z1-19	1.36	0.02	0.14	0.00	0.57	877.78	31.49	870.40	7.88	99%
0906-Z1-20	3.94	0.06	0.29	0.00	0.64	1602.16	26.08	1630.18	14.59	99%
0906-Z1-21	11.41	0.24	0.50	0.01	0.60	2500.00	24.85	2624.08	26.88	97%
0906-Z1-22	4.72	0.08	0.35	0.00	0.46	1594.45	31.48	1914.92	12.40	92%
0906-Z1-23	1.91	0.04	0.17	0.00	0.39	1177.47	50.92	1036.71	8.21	95%
0906-Z1-24	2.22	0.05	0.18	0.00	0.43	1358.33	40.28	1091.59	9.89	91%
0906-Z1-25	1.36	0.03	0.15	0.00	0.43	857.40	48.15	873.64	8.28	99%
0906-Z1-26	1.55	0.03	0.16	0.00	0.62	921.91	33.33	959.38	9.86	99%
0906-Z1-27	1.16	0.03	0.12	0.00	0.60	927.78	69.60	750.35	12.07	95%
0906-Z1-28	1.45	0.02	0.15	0.00	0.46	916.67	27.78	905.42	5.40	99%
0906-Z1-29	1.72	0.04	0.17	0.00	0.45	998.15	46.30	1023.18	10.43	99%
0906-Z1-30	10.74	0.18	0.48	0.00	0.60	2477.46	24.69	2520.02	21.48	99%
0906-Z1-31	1.78	0.03	0.17	0.00	0.66	1053.71	35.19	1032.17	11.54	99%
0906-Z1-32	1.39	0.03	0.15	0.00	0.64	864.81	34.42	891.58	10.94	99%
0906-Z1-33	4.01	0.08	0.29	0.00	0.61	1609.26	31.17	1652.61	17.64	98%
0906-Z1-34	13.58	0.23	0.53	0.01	0.61	2708.95	22.69	2730.46	22.65	99%
0906-Z1-35	2.07	0.04	0.19	0.00	0.55	1127.79	33.34	1142.00	10.52	99%
0906-Z1-36	1.35	0.02	0.14	0.00	0.67	847.83	31.48	871.24	9.80	99%
0906-Z1-37	1.31	0.02	0.14	0.00	0.53	850.00	35.18	849.74	8.09	99%
0906-Z1-38	1.32	0.03	0.14	0.00	0.52	894.45	37.81	839.14	7.94	98%
0906-Z1-39	11.07	0.17	0.48	0.00	0.62	2524.07	23.30	2528.31	20.26	99%
0906-Z1-40	11.00	0.19	0.48	0.01	0.59	2504.63	25.93	2538.86	21.84	99%
0906-Z1-41	4.47	0.09	0.30	0.00	0.55	1738.89	35.03	1710.16	17.41	99%
0906-Z1-42	1.39	0.03	0.15	0.00	0.69	900.00	37.04	879.60	13.22	99%
0906-Z1-43	1.48	0.05	0.15	0.00	0.37	905.56	72.23	926.69	10.64	99%
0906-Z1-44	6.83	0.15	0.37	0.00	0.56	2200.00	27.93	2033.38	21.56	97%
0906-Z1-45	1.42	0.02	0.14	0.00	0.45	953.70	29.63	870.55	6.19	97%
0906-Z1-46	7.90	0.13	0.41	0.00	0.63	2216.36	22.68	2217.55	19.46	99%
0906-Z1-47	1.28	0.04	0.14	0.00	0.39	864.81	104.63	835.28	9.67	99%
0906-Z1-48	6.26	0.13	0.37	0.00	0.50	1988.58	33.33	2030.49	18.29	99%
0906-Z1-49	1.32	0.04	0.14	0.00	0.41	875.93	54.78	846.21	8.85	99%
0906-Z1-50	1.40	0.03	0.15	0.00	0.55	883.33	30.56	887.32	9.26	99%
0906-Z1-51	1.83	0.05	0.18	0.00	0.50	1075.93	45.37	1049.03	12.21	99%
0906-Z1-52	12.05	0.19	0.50	0.01	0.70	2609.26	22.22	2604.84	23.41	99%
0906-Z1-53	1.40	0.03	0.15	0.00	0.55	883.33	30.56	890.24	8.27	99%
0906-Z1-54	5.23	0.08	0.33	0.00	0.56	1857.41	25.93	1851.28	14.33	99%
0906-Z1-55	10.59	0.18	0.47	0.00	0.60	2468.82	25.93	2503.09	21.81	99%
0906-Z1-56	3.09	0.05	0.25	0.00	0.58	1438.89	61.58	1419.08	11.90	99%
0906-Z1-57	7.60	0.11	0.37	0.00	0.59	2323.77	22.38	2033.33	15.11	92%
0906-Z1-58	10.67	0.16	0.47	0.00	0.62	2499.08	23.15	2481.48	19.77	99%
0906-Z1-59	3.81	0.06	0.28	0.00	0.66	1588.58	24.22	1592.56	14.30	99%
0906-Z1-60	5.37	0.09	0.34	0.00	0.65	1857.41	27.01	1895.49	17.94	99%
0906-Z1-61	3.09	0.05	0.25	0.00	0.62	1431.49	31.02	1427.46	13.41	99%
0906-Z1-62	11.30	0.19	0.48	0.01	0.64	2553.70	23.77	2532.30	22.57	99%
0906-Z1-63	1.40	0.03	0.15	0.00	0.50	901.85	48.15	883.48	9.26	99%
0906-Z1-64	1.38	0.03	0.15	0.00	0.54	879.63	37.04	875.44	8.32	99%
0906-Z1-65	1.71	0.03	0.17	0.00	0.48	999.69	37.81	1017.22	8.29	99%
Sample 041003-D1: Metasandstone			**GPS: N25°23'55'', E109°06'13''**							
1003-Z1-01	3.13	0.07	0.25	0.00	0.50	1433.34	39.51	1448.71	14.95	99%
1003-Z1-02	1.24	0.04	0.14	0.00	0.41	820.37	60.34	819.41	9.59	99%
1003-Z1-03	11.11	0.17	0.48	0.00	0.42	2521.30	24.07	2540.77	13.39	99%
1003-Z1-04	1.49	0.03	0.15	0.00	0.54	940.43	31.48	918.53	7.91	99%
1003-Z1-05	2.32	0.04	0.21	0.00	0.56	1212.96	26.85	1219.42	11.23	99%
1003-Z1-06	11.07	0.20	0.48	0.00	0.47	2522.22	28.09	2546.65	17.61	99%
1003-Z1-07	3.89	0.08	0.29	0.00	0.50	1598.15	34.88	1619.79	14.83	99%
1003-Z1-08	1.80	0.14	0.18	0.00	0.26	1032.41	193.36	1071.62	19.04	97%
1003-Z1-09	1.50	0.03	0.15	0.00	0.53	931.48	39.97	928.88	9.32	99%
1003-Z1-10	3.98	0.06	0.29	0.00	0.55	1629.32	25.93	1629.28	12.08	99%
1003-Z1-11	1.53	0.02	0.16	0.00	0.59	964.81	4.63	933.23	7.70	98%
1003-Z1-12	4.42	0.06	0.31	0.00	0.50	1699.08	22.69	1727.96	10.33	99%
1003-Z1-13	3.29	0.05	0.25	0.00	0.62	1494.75	24.07	1459.59	11.12	98%
1003-Z1-14	10.52	0.13	0.45	0.00	0.63	2538.58	18.52	2400.19	16.33	96%
1003-Z1-15	4.25	0.06	0.29	0.00	0.53	1742.59	25.46	1632.40	10.64	96%
1003-Z1-16	1.50	0.04	0.16	0.00	0.38	905.56	56.48	935.13	8.70	99%
1003-Z1-17	4.35	0.07	0.30	0.00	0.60	1722.22	26.85	1691.16	14.80	99%
1003-Z1-18	4.42	0.07	0.31	0.00	0.61	1695.37	25.16	1728.57	14.84	99%
1003-Z1-19	1.31	0.03	0.14	0.00	0.42	857.40	50.77	847.10	8.33	99%
1003-Z1-20	3.99	0.07	0.29	0.00	0.56	1609.26	23.61	1648.88	14.33	99%

Continued Table 1

Analysis	Corrected ratios					Corrected ages (Ma)				Concordance limit
	$^{207}Pb/^{206}Pb$		$^{206}Pb/^{238}U$		rho	$^{207}Pb/^{206}Pb$		$^{206}Pb/^{238}U$		
	± 1σ		± 1σ			± 1σ		± 1σ		
1003-Z1-21	1.35	0.03	0.15	0.00	0.55	831.48	33.33	877.28	8.38	98%
1003-Z1-22	5.45	0.10	0.34	0.00	0.61	1899.08	28.86	1885.80	17.33	99%
1003-Z1-23	10.25	0.15	0.46	0.00	0.61	2478.70	20.99	2423.76	17.51	98%
1003-Z1-24	1.58	0.04	0.16	0.00	0.44	995.99	46.30	946.39	9.56	98%
1003-Z1-25	2.04	0.03	0.19	0.00	0.61	1121.91	24.08	1128.34	8.77	99%
1003-Z1-26	1.32	0.02	0.14	0.00	0.52	833.02	167.60	860.28	7.12	99%
1003-Z1-27	4.38	0.07	0.31	0.00	0.55	1676.23	25.46	1726.61	13.21	98%
1003-Z1-28	1.34	0.03	0.14	0.00	0.41	836.72	42.59	870.16	6.85	99%
1003-Z1-29	1.44	0.02	0.15	0.00	0.50	909.26	33.33	899.98	7.00	99%
1003-Z1-30	3.14	0.06	0.25	0.00	0.55	1431.49	31.33	1445.86	13.08	99%
1003-Z1-31	1.29	0.02	0.14	0.00	0.61	833.33	27.78	848.52	6.94	99%
1003-Z1-32	2.72	0.04	0.23	0.00	0.70	1309.26	22.22	1344.95	12.57	99%
1003-Z1-33	1.63	0.03	0.17	0.00	0.60	969.44	36.11	986.50	8.76	99%
1003-Z1-34	3.80	0.05	0.28	0.00	0.66	1557.72	26.39	1612.37	12.82	98%
1003-Z1-35	1.95	0.04	0.19	0.00	0.60	1083.34	35.34	1105.61	11.09	99%
1003-Z1-36	1.51	0.02	0.16	0.00	0.60	927.78	25.93	931.31	7.64	99%
1003-Z1-37	1.82	0.06	0.17	0.00	0.44	1107.10	43.67	1006.09	12.85	95%
1003-Z1-38	1.32	0.02	0.14	0.00	0.53	864.81	30.56	844.81	5.70	99%
1003-Z1-39	5.41	0.08	0.35	0.00	0.65	1839.20	23.00	1920.57	16.81	98%
1003-Z1-40	1.54	0.03	0.16	0.00	0.46	970.06	42.59	936.99	8.82	98%
1003-Z1-41	4.43	0.07	0.31	0.00	0.65	1701.85	23.77	1724.35	14.43	99%
1003-Z1-42	14.79	0.18	0.54	0.00	0.67	2804.63	23.30	2784.32	18.79	99%
1003-Z1-43	2.08	0.03	0.19	0.00	0.57	1166.67	25.92	1129.55	7.95	98%
1003-Z1-44	1.68	0.03	0.16	0.00	0.52	1055.56	31.48	966.96	8.95	96%
1003-Z1-45	4.41	0.07	0.30	0.00	0.64	1722.22	25.92	1706.27	14.65	99%
1003-Z1-46	6.38	0.09	0.37	0.00	0.70	2014.50	20.52	2031.88	17.33	99%
1003-Z1-47	1.70	0.04	0.16	0.00	0.45	1101.85	46.76	968.81	9.39	95%
1003-Z1-48	3.63	0.04	0.27	0.00	0.58	1590.74	21.14	1522.71	9.74	97%
1003-Z1-49	4.32	0.06	0.29	0.00	0.65	1728.70	20.37	1662.81	12.51	97%
1003-Z1-50	4.53	0.06	0.31	0.00	0.69	1736.11	21.61	1728.62	14.98	99%
1003-Z1-51	10.34	0.16	0.45	0.00	0.65	2516.67	22.68	2398.35	19.57	97%
1003-Z1-52	5.12	0.09	0.32	0.00	0.59	1887.35	27.78	1793.47	15.58	97%
1003-Z1-53	11.64	0.18	0.45	0.00	0.60	2720.38	21.15	2389.90	18.30	92%
1003-Z1-54	1.63	0.03	0.17	0.00	0.54	968.52	5.56	987.35	9.30	99%
1003-Z1-55	4.50	0.07	0.31	0.00	0.62	1738.89	23.77	1722.48	14.36	99%
1003-Z1-56	4.84	0.07	0.32	0.00	0.58	1818.21	23.61	1767.33	13.07	98%
1003-Z1-57	4.33	0.07	0.30	0.00	0.57	1683.34	25.93	1708.18	14.07	99%
1003-Z1-58	7.52	0.12	0.41	0.00	0.51	2150.00	25.93	2200.98	15.46	98%
1003-Z1-59	11.55	0.20	0.50	0.00	0.54	2521.91	23.92	2621.58	20.57	97%
1003-Z1-60	3.26	0.07	0.26	0.00	0.48	1421.91	36.73	1509.49	13.20	97%
1003-Z1-61	4.48	0.10	0.31	0.00	0.45	1709.26	38.43	1739.33	15.74	99%
1003-Z1-62	3.88	0.07	0.29	0.00	0.49	1575.93	29.17	1632.72	12.24	98%
1003-Z1-63	4.43	0.07	0.31	0.00	0.53	1684.26	25.47	1741.76	12.77	98%
1003-Z1-64	2.80	0.05	0.23	0.00	0.51	1350.00	35.34	1357.14	10.98	99%
1003-Z1-65	4.87	0.07	0.33	0.00	0.62	1718.21	22.53	1858.76	15.32	96%
Sample 040808-D1: Andesite,	**755.8±4.8 Ma (n=10)**				**GPS: N25°13'51'', E109°12'23''**					
0808-Z1-01	1.25	0.03	0.13	0.00	0.45	853.70	149.08	814.46	8.35	98%
0808-Z1-02	1.15	0.04	0.13	0.00	0.49	724.08	61.11	798.20	12.54	97%
0808-Z1-03	1.36	0.03	0.14	0.00	0.51	861.11	45.22	871.71	9.57	99%
0808-Z1-04	1.10	0.05	0.13	0.00	0.34	522.26	119.43	771.11	10.27	97%
0808-Z1-05	1.23	0.04	0.13	0.00	0.32	842.59	66.67	805.35	7.69	98%
0808-Z1-06	1.13	0.03	0.13	0.00	0.43	753.71	247.22	772.16	7.21	99%
0808-Z1-07	1.14	0.04	0.13	0.00	0.37	744.14	41.66	785.80	8.91	98%
0808-Z1-08	1.33	0.05	0.15	0.00	0.29	809.26	88.89	879.77	9.98	97%
0808-Z1-09	1.27	0.06	0.14	0.00	0.28	855.55	101.85	830.96	10.56	99%
0808-Z1-10	1.16	0.03	0.13	0.00	0.47	746.30	250.00	794.34	9.12	98%
0808-Z1-11	1.16	0.03	0.13	0.00	0.44	694.46	41.66	812.47	7.67	96%
0808-Z1-12	1.23	0.04	0.14	0.00	0.40	746.30	59.25	835.85	8.92	97%
0808-Z1-13	1.22	0.03	0.13	0.00	0.46	805.56	61.11	813.36	9.80	99%
0808-Z1-14	1.10	0.02	0.12	0.00	0.50	738.90	35.18	754.49	6.07	99%
0808-Z1-15	1.11	0.04	0.13	0.00	0.38	744.14	41.66	765.80	10.10	99%
0808-Z1-16	1.20	0.04	0.14	0.00	0.39	764.82	63.73	816.88	8.96	98%
0808-Z1-17	1.44	0.10	0.15	0.00	0.23	907.10	175.92	928.55	13.54	97%
0808-Z1-18	1.18	0.03	0.13	0.00	0.42	768.52	47.22	800.69	7.67	98%
0808-Z1-19	1.14	0.04	0.13	0.00	0.37	744.45	72.99	788.68	9.44	98%
0808-Z1-20	1.32	0.03	0.14	0.00	0.39	836.72	46.30	854.70	7.06	99%
0808-Z1-21	1.19	0.03	0.12	0.00	0.39	900.00	58.49	758.48	7.90	95%
0808-Z1-22	1.21	0.04	0.13	0.00	0.35	809.26	64.81	801.92	8.18	99%
0808-Z1-23	1.21	0.03	0.13	0.00	0.38	798.15	46.29	804.11	6.39	99%

Continued Table 1

Analysis	Corrected ratios					Corrected ages (Ma)				Concordance limit
	$^{207}Pb/^{206}Pb$	± 1σ	$^{206}Pb/^{238}U$	± 1σ	rho	$^{207}Pb/^{206}Pb$	± 1σ	$^{206}Pb/^{238}U$	± 1σ	
0808-Z1-24	1.27	0.05	0.14	0.00	0.44	840.43	84.10	840.55	12.96	99%
0808-Z1-25	15.86	0.25	0.55	0.00	0.52	2902.78	24.54	2807.23	18.78	97%
0808-Z1-26	1.36	0.06	0.15	0.00	0.29	875.93	90.74	878.70	10.55	99%
0808-Z1-27	1.18	0.02	0.13	0.00	0.50	783.34	47.22	789.91	7.58	99%
0808-Z1-28	1.27	0.05	0.14	0.00	0.35	820.37	75.00	836.25	9.94	99%
0808-Z1-29	1.32	0.03	0.14	0.00	0.55	835.18	42.59	862.49	9.61	99%
0808-Z1-30	1.25	0.03	0.14	0.00	0.34	1200.00	50.00	827.05	6.51	99%
0808-Z1-31	1.10	0.03	0.12	0.00	0.37	764.82	62.96	754.22	7.35	99%
0808-Z1-32	1.27	0.03	0.14	0.00	0.42	816.67	48.15	833.35	7.43	99%
0808-Z1-33	1.28	0.04	0.14	0.00	0.34	783.34	60.03	851.96	8.04	98%
0808-Z1-34	1.29	0.03	0.14	0.00	0.45	838.89	48.15	843.71	8.04	99%
0808-Z1-35	1.65	0.10	0.13	0.00	0.25	1387.04	110.19	800.82	12.17	78%
0808-Z1-36	1.39	0.04	0.15	0.00	0.43	872.22	52.93	889.04	9.54	99%
0808-Z1-37	1.14	0.03	0.13	0.00	0.39	768.52	51.69	768.28	7.83	99%
0808-Z1-38	1.47	0.06	0.15	0.00	0.35	950.00	83.34	916.05	11.20	99%
0808-Z1-39	1.31	0.03	0.14	0.00	0.43	872.22	43.52	836.56	8.37	98%
0808-Z1-40	1.05	0.04	0.12	0.00	0.54	705.57	300.92	749.09	15.84	97%
0808-Z1-41	1.51	0.05	0.15	0.00	0.33	1064.82	68.52	877.19	8.33	93%
0808-Z1-42	1.36	0.03	0.14	0.00	0.51	877.78	40.74	869.77	8.83	99%
0808-Z1-43	1.24	0.03	0.14	0.00	0.49	772.23	44.44	828.03	10.26	98%
0808-Z1-44	1.13	0.03	0.13	0.00	0.37	746.30	50.00	768.93	6.33	99%
0808-Z1-45	1.28	0.03	0.14	0.00	0.48	820.37	58.18	841.94	10.36	99%
0808-Z1-46	1.21	0.04	0.13	0.00	0.37	900.00	79.63	781.87	9.30	97%
0808-Z1-47	1.37	0.03	0.15	0.00	0.47	877.78	38.74	873.36	8.41	99%
0808-Z1-48	1.11	0.10	0.12	0.00	0.18	679.64	135.17	747.34	11.65	98%
0808-Z1-49	1.11	0.04	0.12	0.00	0.38	775.93	74.99	757.35	8.97	99%
0808-Z1-50	1.11	0.02	0.12	0.00	0.35	768.52	46.29	753.88	5.35	99%
0808-Z1-51	1.22	0.03	0.13	0.00	0.37	1200.00	48.14	807.98	6.75	99%
0808-Z1-52	1.24	0.05	0.13	0.00	0.37	820.37	75.92	813.22	11.09	99%
0808-Z1-53	1.30	0.04	0.14	0.00	0.34	835.18	74.07	856.78	9.08	98%
0808-Z1-54	1.14	0.02	0.13	0.00	0.42	731.49	43.36	785.17	6.47	98%
0808-Z1-55	1.17	0.03	0.13	0.00	0.36	788.58	63.88	784.64	7.54	99%
0808-Z1-56	1.10	0.03	0.12	0.00	0.46	750.01	48.15	756.13	7.50	99%
0808-Z1-57	1.30	0.04	0.14	0.00	0.45	853.70	54.48	843.43	10.13	99%
0808-Z1-58	1.35	0.04	0.14	0.00	0.38	864.81	137.97	870.08	9.02	99%
0808-Z1-59	1.10	0.03	0.12	0.00	0.41	744.45	40.58	758.68	6.79	99%
0808-Z1-60	1.07	0.02	0.12	0.00	0.50	742.60	35.18	734.36	6.43	99%
0808-Z1-61	1.31	0.05	0.14	0.00	0.31	900.00	74.08	838.73	9.01	98%
0808-Z1-62	1.17	0.02	0.13	0.00	0.53	805.56	33.33	780.29	6.81	99%
0808-Z1-63	1.19	0.03	0.13	0.00	0.42	798.15	46.29	796.73	7.16	99%
0808-Z1-64	1.31	0.03	0.14	0.00	0.36	875.93	43.52	840.20	5.54	98%
0808-Z1-65	1.15	0.02	0.13	0.00	0.51	792.28	42.59	775.39	7.44	99%
Sample 041001-D1: Granite, 814.4±4.5 Ma (n=10) GPS: N25°25'29'', E109°07'46''										
1001-Z1-01	1.33	0.02	0.15	0.00	0.53	1200.00	33.33	879.98	7.79	97%
1001-Z1-02	1.30	0.02	0.14	0.00	0.53	790.74	33.33	861.99	7.32	97%
1001-Z1-03	1.28	0.02	0.14	0.00	0.45	842.59	35.18	830.56	6.53	99%
1001-Z1-04	1.33	0.02	0.14	0.00	0.53	842.59	33.33	861.56	7.20	99%
1001-Z1-05	1.36	0.02	0.15	0.00	0.60	833.33	33.33	886.91	8.92	98%
1001-Z1-06	1.25	0.02	0.14	0.00	0.50	787.04	33.33	835.56	6.27	98%
1001-Z1-07	1.35	0.02	0.15	0.00	0.61	838.89	33.33	876.70	9.04	98%
1001-Z1-08	1.28	0.02	0.14	0.00	0.57	820.37	31.48	839.74	7.76	99%
1001-Z1-09	1.23	0.02	0.13	0.00	0.50	794.45	35.18	814.96	7.15	99%
1001-Z1-10	1.29	0.02	0.14	0.00	0.59	809.26	30.71	853.11	8.23	98%
1001-Z1-11	1.29	0.02	0.14	0.00	0.51	850.00	33.33	836.70	7.20	99%
1001-Z1-13	1.26	0.02	0.14	0.00	0.53	831.48	35.18	827.81	7.25	99%
1001-Z1-14	1.25	0.02	0.14	0.00	0.57	820.37	31.48	820.52	7.33	99%
1001-Z1-15	2.57	0.08	0.20	0.00	0.67	1438.89	33.18	1172.59	22.37	90%
1001-Z1-16	1.33	0.02	0.14	0.00	0.58	853.70	25.00	858.48	7.56	99%
1001-Z1-17	1.38	0.02	0.15	0.00	0.54	857.40	30.40	885.73	7.17	99%
1001-Z1-18	1.25	0.03	0.14	0.00	0.44	831.48	43.52	817.25	6.94	99%
1001-Z1-19	1.26	0.03	0.14	0.00	0.43	838.89	39.97	820.51	6.79	99%
1001-Z1-20	1.22	0.02	0.14	0.00	0.48	758.95	35.18	828.57	7.08	97%
1001-Z1-21	1.25	0.03	0.13	0.00	0.41	916.67	44.45	784.77	7.60	95%
1001-Z1-22	1.22	0.02	0.13	0.00	0.48	833.33	35.18	802.62	6.64	99%
1001-Z1-23	1.27	0.02	0.14	0.00	0.54	833.33	35.18	832.72	7.98	99%
1001-Z1-24	1.23	0.02	0.13	0.00	0.61	833.33	29.63	809.80	7.25	99%
1001-Z1-25	1.51	0.03	0.16	0.00	0.40	1000.00	38.89	934.46	6.83	99%
1001-Z1-26	1.20	0.02	0.13	0.00	0.56	798.15	37.03	800.73	7.90	99%
1001-Z1-27	1.24	0.03	0.14	0.00	0.47	803.39	48.14	825.25	9.17	99%

Continued Table 1

Analysis	Corrected ratios					Corrected ages (Ma)				Concordance limit
	$^{207}Pb/^{206}Pb$		$^{206}Pb/^{238}U$			$^{207}Pb/^{206}Pb$		$^{206}Pb/^{238}U$		
	± 1σ		± 1σ		rho	± 1σ		± 1σ		
1001-Z1-28	1.30	0.03	0.14	0.00	0.51	840.43	42.59	843.95	9.06	99%
1001-Z1-29	1.24	0.02	0.14	0.00	0.53	816.67	34.41	818.47	7.31	99%
1001-Z1-30	1.24	0.02	0.14	0.00	0.52	833.33	31.48	816.73	6.57	99%
1001-Z1-31	1.24	0.02	0.14	0.00	0.51	790.74	33.33	827.87	7.20	99%
1001-Z1-32	1.39	0.03	0.15	0.00	0.39	833.33	40.74	903.97	6.59	97%
1001-Z1-33	1.41	0.03	0.15	0.00	0.39	820.37	37.03	919.35	6.02	97%
1001-Z1-34	2.49	0.05	0.22	0.00	0.48	1273.76	33.34	1256.90	10.77	99%
Sample 120904-D1: Metasandstone			**GPS: N26°29'03'', E109°13'57''**							
120904-01	0.07	0.00	0.28	0.00	0.41	987.04	43.52	1616.45	11.13	83%
120904-02	0.14	0.00	0.48	0.00	0.42	2202.78	37.66	2514.88	18.60	93%
120904-03	0.13	0.00	0.45	0.00	0.45	2080.55	30.25	2413.47	15.41	92%
120904-04	0.07	0.00	0.17	0.00	0.32	1009.26	53.71	995.81	8.36	99%
120904-05	0.10	0.00	0.30	0.00	0.29	1612.96	39.66	1696.38	10.36	98%
120904-06	0.09	0.00	0.25	0.00	0.38	1411.11	31.95	1418.77	7.48	99%
120904-07	0.08	0.00	0.18	0.01	0.90	1188.89	70.37	1080.65	37.15	99%
120904-08	0.07	0.00	0.15	0.00	0.48	909.26	39.97	918.80	7.74	99%
120904-09	0.09	0.00	0.27	0.00	0.55	1527.79	34.26	1520.32	11.60	99%
120904-10	0.10	0.00	0.30	0.00	0.45	1699.69	27.63	1687.31	9.57	99%
120904-11	0.10	0.00	0.31	0.00	0.40	1694.45	33.18	1720.78	10.77	99%
120904-12	0.11	0.00	0.31	0.00	0.50	1750.92	32.41	1758.05	11.44	99%
120904-13	0.07	0.00	0.14	0.00	0.37	831.48	44.44	844.49	6.30	99%
120904-14	0.08	0.00	0.21	0.00	0.36	1212.96	37.03	1218.08	7.16	99%
120904-15	0.15	0.00	0.43	0.01	0.66	2339.82	23.15	2306.52	24.52	99%
120904-16	0.07	0.00	0.16	0.00	0.36	920.37	44.44	932.94	7.00	99%
120904-17	0.16	0.00	0.48	0.00	0.44	2501.85	30.56	2515.71	16.52	99%
120904-18	0.10	0.00	0.29	0.00	0.42	1636.72	37.65	1656.37	13.22	99%
120904-19	0.07	0.00	0.16	0.00	0.42	946.29	40.74	959.71	7.57	99%
120904-20	0.07	0.00	0.17	0.00	0.43	998.15	36.12	996.68	8.48	99%
120904-21	0.07	0.00	0.14	0.00	0.37	788.89	59.25	830.53	6.90	99%
120904-22	0.08	0.00	0.14	0.00	0.34	1231.48	48.15	855.77	7.11	86%
120904-23	0.10	0.00	0.30	0.00	0.39	1635.18	43.37	1684.46	13.63	99%
120904-24	0.09	0.00	0.25	0.00	0.43	1411.11	49.23	1428.78	14.64	99%
120904-25	0.16	0.00	0.47	0.00	0.39	2445.98	43.52	2478.02	20.91	99%
120904-26	0.17	0.00	0.39	0.01	0.62	2513.27	46.30	2138.23	31.03	91%
120904-27	0.11	0.00	0.33	0.00	0.40	1768.83	40.74	1815.19	13.95	99%
120904-28	0.16	0.00	0.49	0.00	0.39	2505.86	44.91	2553.67	18.75	99%
120904-29	0.08	0.00	0.24	0.00	0.42	1283.34	46.30	1375.88	11.02	98%
120904-30	0.15	0.00	0.45	0.02	0.89	2392.28	40.12	2398.00	90.08	99%
120904-31	0.11	0.00	0.35	0.00	0.61	1744.13	31.64	1918.49	18.38	95%
120904-32	0.07	0.00	0.17	0.00	0.31	1016.67	45.53	1034.24	7.14	99%
120904-33	0.10	0.00	0.30	0.00	0.40	1705.87	29.63	1705.85	9.72	99%
120904-34	0.07	0.00	0.14	0.00	0.30	861.11	141.67	852.99	6.85	99%
120904-35	0.11	0.00	0.33	0.01	0.86	1835.19	30.87	1837.62	30.98	99%
120904-36	0.08	0.00	0.20	0.00	0.27	1151.55	57.41	1152.27	7.47	99%
120904-37	0.10	0.00	0.30	0.00	0.42	1687.97	30.10	1709.04	10.51	99%
120904-38	0.07	0.00	0.16	0.00	0.35	947.22	43.68	940.58	6.42	99%
120904-39	0.07	0.00	0.14	0.00	0.32	842.59	64.81	840.53	7.34	99%
120904-40	0.10	0.00	0.30	0.00	0.38	1700.00	36.88	1705.20	11.38	99%
120904-41	0.10	0.00	0.27	0.00	0.43	1676.23	33.80	1544.47	12.07	96%
120904-42	0.07	0.00	0.16	0.00	0.34	950.00	44.44	945.65	6.47	99%
120904-43	0.07	0.00	0.15	0.00	0.32	1000.00	81.48	896.27	10.51	99%
120904-44	0.11	0.00	0.34	0.00	0.17	1861.12	73.92	1880.88	12.02	99%
120904-45	0.07	0.00	0.14	0.00	0.31	838.89	52.78	831.64	6.33	99%
120904-46	0.10	0.00	0.33	0.00	0.46	1705.56	31.95	1829.94	13.80	97%
120904-47	0.07	0.00	0.18	0.00	0.32	1061.12	64.04	1060.36	9.42	99%
120904-48	0.17	0.00	0.49	0.00	0.48	2557.10	34.88	2557.50	21.40	99%
120904-49	0.16	0.00	0.47	0.00	0.42	2465.74	32.72	2479.80	16.59	99%
120904-50	0.18	0.00	0.51	0.00	0.45	2649.70	29.01	2665.97	19.00	99%
120904-51	0.10	0.00	0.29	0.00	0.38	1599.08	37.80	1631.91	11.02	99%
120904-52	0.18	0.00	0.47	0.00	0.39	2680.56	31.02	2464.61	14.90	95%
120904-53	0.11	0.00	0.31	0.00	0.41	1742.28	29.48	1739.76	9.58	99%
120904-54	0.12	0.00	0.34	0.00	0.45	1894.45	29.63	1909.23	12.06	99%
120904-55	0.08	0.01	0.21	0.00	0.15	1255.24	121.45	1244.90	12.10	99%
120904-56	0.07	0.00	0.15	0.00	0.40	920.37	40.74	923.20	6.43	99%
120904-57	0.11	0.00	0.29	0.00	0.26	1855.25	50.00	1651.99	10.02	93%
120904-58	0.11	0.00	0.31	0.00	0.41	1742.59	31.17	1746.59	10.68	99%
120904-59	0.07	0.00	0.14	0.00	0.40	864.81	42.59	871.44	6.45	99%
120904-60	0.11	0.00	0.31	0.00	0.42	1750.92	31.48	1746.01	11.65	99%

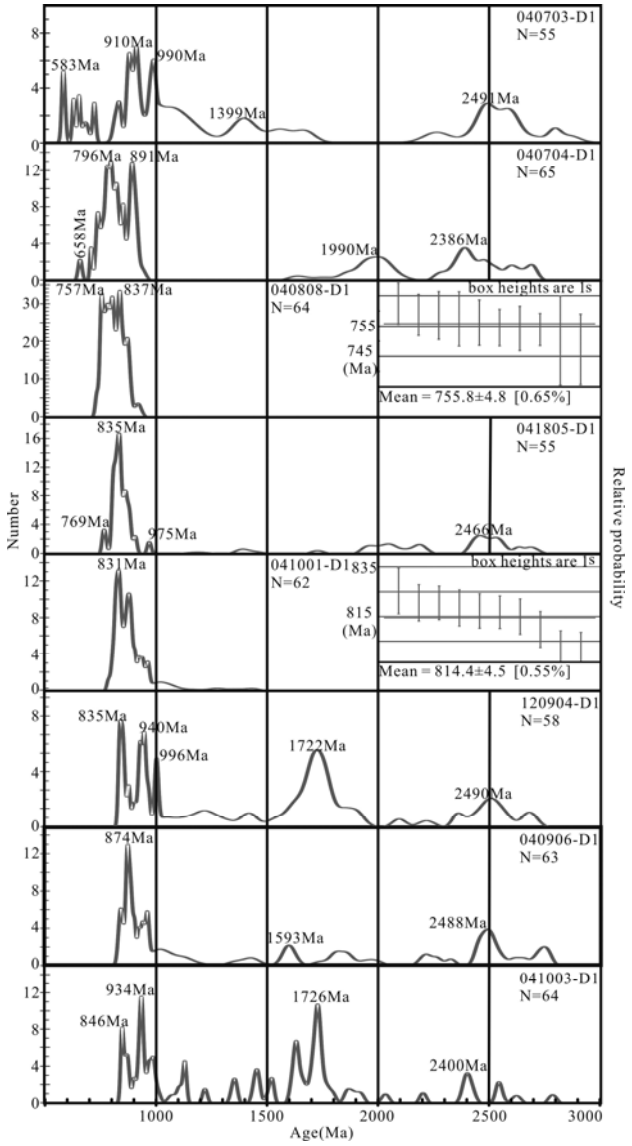


Fig. 8. Relative probability plots of detrital zircon U–Pb ages (with concordance of 90–110%) for a sample from the different strata near the Yuanbaoshan region. Two igneous samples (040808–D1and 041001–D1) are plotted on an average age diagram using the youngest age group.

are shown in Table 2. The plateau ages (quoted at ±2σ) and $^{40}Ar/^{36}Ar$ versus $^{39}Ar/^{36}Ar$ and $^{36}Ar/^{40}Ar$ versus $^{39}Ar/^{40}Ar$ isochron diagrams were defined using the ISOPLOT software (Ludwig, 2001).

4.2 Zircon U–Pb ages

Results for 185 spot analyses on the detrital zircons from the Sibao Group (sample 041003–D1, 040906–D1 and 120904–D1) are plotted in Figure 8. The age spectrum of the three samples is broadly similar, and the ages are combined to represent a preliminary detrital zircon fingerprint for the metasediments of the Sibao Group. Age populations occur mainly between 830 and 1000 Ma, with a peak at 835, 846, 874, 934 and 996 Ma. In addition, age relative probability spectrums show ca. 1593–1726 Ma and ca. 2400–2500 Ma peaks (Fig. 8). The youngest zircon age peak is 835 Ma, derived from sample 120904–D1. Thus, we interpret that the Sibao Group is younger than ~835 Ma (Fig. 8). The Yuanbaoshan granite that intruded the Sibao Group has a youngest average age of 814.4±4.5 Ma, confining the upper age limit of the Sibao Group (sample 041001–D1) (Fig. 8).

Detrital zircon grains from the Danzhou Group (sample 041805–D1) are dominated by a single major age population peak at 835 Ma, with four other distinctive peaks at 769, 975 and 2466 Ma. This age indicates that the Danzhou Group was deposited after 769 Ma. Furthermore, the Danzhou Group is intercalated with a 755.6±4.8 Ma tuff (Fig. 8, sample 040808–D1).

The detrital zircon age spectra of sample 040704–D1 from the Changan Formation sandstones are dominated by Neoproterozoic detrital grains (650–900 Ma) and have peaks at 658, 796, 891, 1990 and 2386 Ma. This unit must be younger than 658 Ma.

The detrital zircon U–Pb patterns of the Cambrian sandstones 040703–D1 in the southeastern area of the Yuanbaoshan pluton consist of a prominent population at 900–1000 Ma, subordinate populations at 500–600 Ma, and minor population peaks at 1399 and 2491 Ma. Hence, the maximum depositional age of the Cambrian sample is not older than the youngest zircon age of 580 Ma.

4.3 Thermochronology

The $^{40}Ar/^{39}Ar$ analyses were conducted on three mica separates from the Sibao Group at the base of the Danzhou Group (Fig. 9). White mica from sample 120909–D1, a schist exhibiting greenschist facies mineral assemblages, generated a plateau age of 454±2.8 Ma. White mica from sample LGXY12 and sample 1207–4, mylonitic schists, generated a plateau age of 471±4.8 Ma and 494±3.8 Ma, respectively. Because of that $^{40}Ar/^{39}Ar$ ages from these two samples have a scattered plateau age and may be unreliable (Fig. 9), the scatter in ages presented here may reflect the effects of fluid or argon lost during fault reactivation (Harrison et al., 2009).

5 Discussions

5.1 Provenance of sediments in the Yuanbaoshan region

Figure 10 shows the detrital zircon age spectrum for our studies and compares our results to U–Pb ages of detrital zircons from Eastern Australia (Fergusson et al., 2007), Western Australia (Griffin et al., 2004) and the Precambrian sequence of the India Craton (Myrow et al.,

Table 2 ^{40}Ar–^{39}Ar step–heating dating results of the three metasiltstones in the Yuanbaoshan area of southwestern Jiangnan Orogen

120909-D1 white mica	W=13.56 mg		J=0.002486				Total age =453.0 Ma			
T(°C)	$(^{40}Ar/^{39}Ar)_m$	$(^{36}Ar/^{39}Ar)_m$	$(^{37}Ar_0/^{39}Ar)_m$	$(^{38}Ar/^{39}Ar)_m$	^{40}Ar (%)	F	^{39}Ar ($\times10^{-14}$ mol)	^{39}Ar (Cum.) (%)	Age (Ma)	±1σ (Ma)
700	137.9789	0.3547	0	0.1382	24.02	33.1456	0.03	0.07	142.8	9.8
800	126.5627	0.0809	1.6504	0.0258	81.2	102.9045	0.28	0.62	410.9	3.8
850	128.7827	0.0304	0	0.0398	93.02	119.7904	0.35	1.34	470.2	4.3
900	124.2065	0.0215	0	0.0176	94.89	117.8537	1.2	3.77	463.5	4.1
940	119.3469	0.0099	0	0.0147	97.55	116.4278	2.04	7.89	458.6	4.1
980	117.328	0.0084	0	0.0142	97.87	114.8316	4.7	17.39	453	4
1020	115.9442	0.0044	0	0.0134	98.87	114.6334	11.13	39.89	452.3	4
1050	115.439	0.0026	0	0.0129	99.33	114.6706	13.73	67.65	452.5	4
1090	115.7571	0.0035	0	0.0147	99.11	114.7304	8.02	83.87	452.7	4
1130	115.7996	0.003	0	0.0125	99.24	114.922	5.23	94.44	453.3	4
1200	116.0549	0.0014	0	0.0094	99.64	115.6338	1.53	97.54	455.8	4.1
1400	117.4197	0.0064	0	0.017	98.39	115.5325	1.22	100	455.5	4.2

LGXY12 white mica	W=13.09mg		J=0.002488				Total age =444.6Ma			
T(°C)	$(^{40}Ar/^{39}Ar)_m$	$(^{36}Ar/^{39}Ar)_m$	$(^{37}Ar_0/^{39}Ar)_m$	$(^{38}Ar/^{39}Ar)_m$	^{40}Ar (%)	F	^{39}Ar ($\times10^{-14}$ mol)	^{39}Ar (Cum.) (%)	Age (Ma)	±1s (Ma)
700	242.4696	0.7488	0	0	8.74	21.2032	0.01	0.01	93	69
800	107.4167	0.0433	0	0.0201	88.07	94.6067	0.37	0.72	381.3	3.6
850	110.8756	0.0276	0	0.0298	92.63	102.7023	0.72	2.11	410.5	3.7
900	109.9984	0.0223	0	0.0175	94.01	103.4045	1.54	5.07	413	3.7
940	106.4798	0.0082	0	0.0131	97.71	104.0395	2.58	10.04	415.3	3.7
980	106.9859	0.0074	0	0.0139	97.96	104.8033	6.15	21.89	418	3.7
1010	110.0377	0.0071	0	0.0138	98.1	107.9419	3.75	29.12	429.1	3.8
1050	111.3799	0.0046	0	0.013	98.77	110.0124	12.67	53.54	436.5	3.9
1080	113.9621	0.0043	0	0.0136	98.89	112.6986	7.04	67.11	445.9	4
1120	120.3387	0.0064	0	0.014	99.42	118.4318	5.12	76.98	465.9	4.1
1160	123.8565	0.0069	0	0.0134	98.34	121.8063	3.79	84.29	477.5	4.2
1220	122.1536	0.0072	0	0.0141	98.26	120.0232	5.23	98.34	471.4	4.1
1300	126.059	0.0082	0	0.012	98.08	123.6441	2.59	99.38	483.9	4.2
1400	127.1538	0.0151	0	0.0092	96.18	122.6829	0.32	100	480.6	4.3

1207-4	White mica	W=13.94mg		J=0.002485			Total age =497.2Ma			
T(°C)	$(^{40}Ar/^{39}Ar)_m$	$(^{36}Ar/^{39}Ar)_m$	$(^{37}Ar_0/^{39}Ar)_m$	$(^{38}Ar/^{39}Ar)_m$	^{40}Ar (%)	F	^{39}Ar ($\times10^{-14}$ mol)	^{39}Ar (Cum.) (%)	Age (Ma)	±1σ(Ma)
700	136.7173	0.1548	0	0.0115	66.61	91.07	0.05	0.09	368	7.9
800	143.2249	0.1182	0	0.0522	75.61	108.2929	0.12	0.33	429.9	4.5
870	131.6641	0.0395	0	0.0199	91.13	119.9857	1.19	2.72	478.8	4.2
900	128.0946	0.0202	0	0.0176	95.35	122.1331	0.76	4.25	478.2	4.2
940	129.2957	0.0149	0	0.014	96.6	124.8996	1.62	7.49	487.6	4.3
980	133.6418	0.0118	0	0.0144	97.39	130.1601	4.15	15.81	505.6	4.4
1020	134.5615	0.008	0.8523	0.0138	98.29	132.3484	9.8	35.45	513	4.5
1050	126.2565	0.003	0	0.0129	99.28	125.3521	11.38	58.27	489.2	4.3
1080	128.5612	0.0119	0	0.0143	97.25	125.026	4.75	67.79	488.1	4.3
1130	129.6379	0.0065	0	0.0135	98.52	127.7165	3.67	75.14	497.3	4.3
1190	130.6031	0.0055	0	0.0135	98.75	128.9693	4.93	85.03	501.5	4.4
1250	128.3034	0.003	0	0.0128	99.3	127.4022	7.16	99.39	496.2	4.3
1320	139.1649	0.0243	0	0.01	94.83	131.9747	0.2	99.79	511.7	4.7
1400	159.553	0.0843	0	0.0216	84.38	134.6286	0.1	100	520.6	5.4

Note: The subscript m in the table represents the isotope ratio measured in the sample. $F=^{40}Ar/^{39}Ar$, is the ratio of radiogenic Argon40 and Argon39

2010). Detrital age spectrum of the Sibao Group show large population at ca. 2500 Ma, 1726 Ma, 914 Ma, 874 Ma and 835 Ma. Based on comparing detrital zircon age data, it could have been sourced from the eroded Yangtze Block in the western Jiangnan Ocean, the India Craton, or Western Australia (Fig. 10). This conclusion agrees with those of Bruguier et al. (1997), who proposed that zircon ages of the SCC have been derived from sources within Australia or from India along the northern margin of Rodinia (Ma et al., 2016). Based on synthetic analyses on available zircon U–Pb ages and Hf isotopes, paleomagnetic data and tectono–stratigraphic records, there was a close relationship between South China and India during the amalgamation of the supercontinent Rodinia (Wang et al., 2013a).

Detrital zircon age peaks of the Danzhou Group shifted the youngest age peak from ca. 835 Ma to ca. 769 Ma and contained abundant 800–850 Ma detrital zircons (Fig. 10). The detrital zircon distribution spectrums of the Danzhou Group, involving syndepositional zircons, suggest a provenance from the Neoproterozoic basement sedimentary sequences along with a mixture of local Neoproterozoic subduction–related felsic granitoids (Fig. 10), and possible recycled materials from the interior of the Yangtze Block (Yan et al., 2015). Although the Changan Formation contains younger detrital zircons

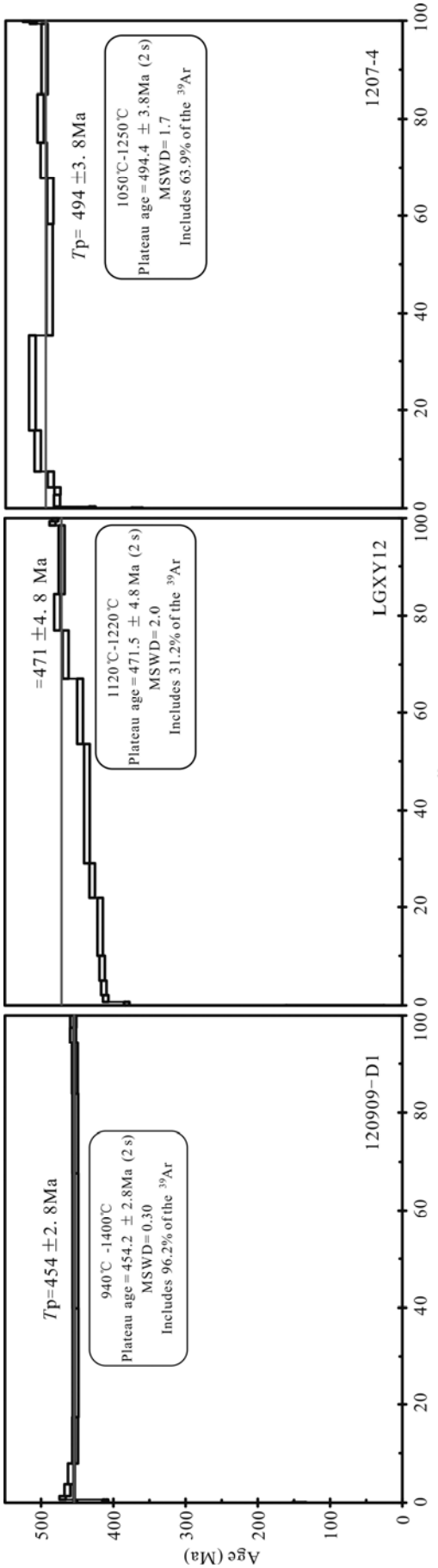


Fig. 9. White mica $^{40}Ar/^{39}Ar$ analyses for the metasiltstone in the Yuanbaoshan region of the southwestern JO.

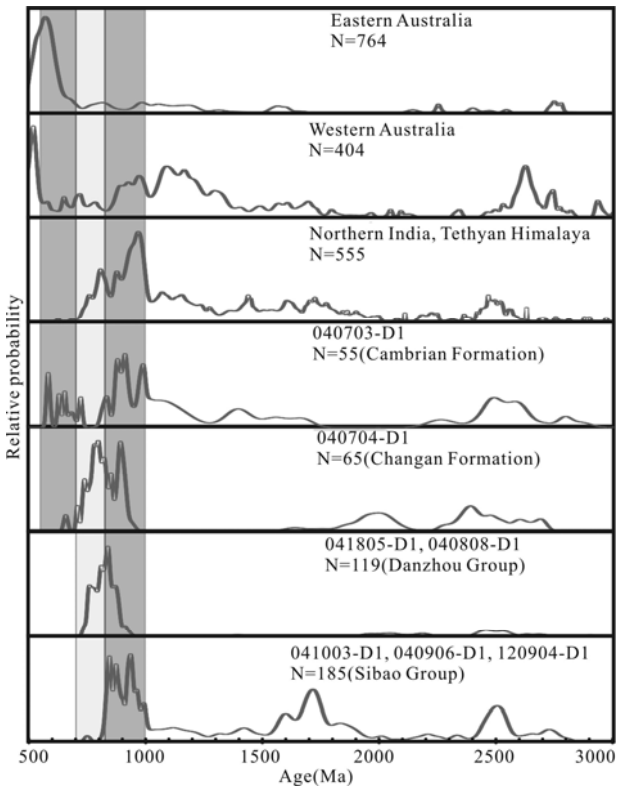


Fig.10. Detrital zircon age distributions for exposed rocks from the Yuanbaoshan region.
From bottom to top: the Sibao Group, Danzhou Group, Changan Formation and Cambrian Formation. Eastern Australia, Western Australia, northern India and Tethyan Himalaya are also displayed for comparison with the SCC. Data compiled from Fergusson et al. (2007) for Eastern Australia; Griffin et al. (2004) for Western Australia; Myrow et al., (2010) for northern India and Tethyan Himalaya.

compared with the Danzhou Group, it has a similar detrital zircon spectrum as the Danzhou Group, which indicates a similar source region for these two units (Fig. 10). The upper Changan Formation contains abundant 750–900 Ma detrital ages that are possibly derived from a local source of the JO and united SCC (Fig. 10).

The detrital zircon age spectrum for the Cambrian strata (sample 040703–D1) includes ca. 550–700, 900–1000, 1400 and 2500 Ma peaks that show similar detrital zircon trait with the northern India (Fig. 10). These age peaks were widespread across the East Gondwana cratons of Australia and India (Fitzsimons, 2000; Boger et al., 2001; Xu et al., 2013). A sharp change in the detrital zircon age spectrum of the Cambrian strata from older strata may indicate that the collision between the SCC and different provinces and continents at that time (Fig. 10). Due to ca. 550 Ma detrital ages are widely occurred on the Indian continental, the SCC probably has a Gondwana affinity and hence it was possibly adjacent to northwestern Gondwana in the Middle Paleozoic (Chen et al., 2016). These belts were juxtaposed during the assembly of Gondwana in the Late Neoproterozoic–Early Cambrian,

forming the Pan–African orogens (Fitzsimons, 2000; Cawood and Buchan, 2007).

5.2 Tectonic evolution of the Yuanbaoshan region

The exposed geological units are the foundation of the regional geology reconstruction. Below, we summarize our new structural and thermogeochronology evidence, as well as previously published ones, which offer more constraints on the tectonic evolution of the Yuanbaoshan region and help to understand the geological evolution of the JO and the SCC.

In our mapping area, the oldest Sibao Group has a maximum depositional age ca. 835 Ma and is intruded by the ca. 815 Ma Yuanbaoshan granite (Fig. 8) (Yao et al., 2014c). However, it contains much older (1000–850 Ma) (ultra)mafic blocks (Lin et al., 2015), which is a typical subduction mélange trait (Fig. 5g–h). These results imply an old suture zone was present in the Yuanbaoshan region before the ca. 815 Ma Yuanbaoshan granitic intrusions. The Sibao Group records one early phase of deformation, which occurred during subduction of the old Jiangnan Ocean. Moreover, top–to–the–east shearing indicators probably indicate westward subduction of the oceanic lithosphere (Fig. 4). The Yuanbaoshan granite pluton is a typical S–type granite emplaced ca. 830–820 Ma within a syncollisional tectonic setting (Yao et al., 2014c). These results suggest closure of this ocean and the collision between the Yangtze and Cathyasia Blocks occurred between approximately ca. 835 Ma and ca. 815 Ma.

Both the metamorphosed Sibao Group and Yuanbaoshan granite are overlain by the post collision Danzhou Group, which confirms that the Yuanbaoshan granite experienced exhumation before the overlying unconformity (Fig. 4). Continental–scale extension induced abundant volcanic eruptions or igneous intrusions that are recorded in the Danzhou Group (Fig. 7d). These events are also supported by the detrital zircon ages from the Danzhou Group, which contained abundant coeval depositional zircons (Fig. 8). The extension led to basin deposition, which lasted from ca. 800 Ma until the Cambrian, because a similar detrital zircon age spectrum is present in the Changan Formation (Fig. 10). This late stage extensional event did not trigger more volcanism, excluding the formation of a new ocean during this continental extension event. This conclusion is similar to the intra–continental rifting model (Yu et al., 2016; Yan et al., 2017).

The newly–formed basin finally closed due to intra–continental collision (Shi et al., 2015). In the Yuanbaoshan area, a north–south–striking positive flower structure was formed by the intra–continental collision and exhumed the former deeply–buried Sibao Group and Yuanbaoshan granite, which may have experienced high–greenschist metamorphism (Fig. 7h). This exhumation stage occurred approximately 450 Ma and may have continued until 400 Ma (Fig. 9) (Zhang et al., 2016a). These results are supported by the second phase of deformation that involved the Ordovician strata but did not affect the Devonian units (Fig. 4). The second phase of deformation is the dominant one in our study area that influenced both the Sibao and Danzhou Groups. The 3D profile reconstructions illustrate top–to–the–east shearing in the Yuanbaoshan and Longsheng area, whereas top–to–the–west shearing around the Sangfang granite indicates a positive flower structure was present between the Yuanbaoshan and Sangfang plutons. Furthermore, the deep extension of the flower structure may have been an inherited Neoproterozoic suture relic, which was a potential weak zone.

5.3 Comparing the Yuanbaoshan region with the eastern JO and general tectonic evolution of the JO

There are two debated hypotheses for the location of the SCC during the Proterozoic, whether it was within or on the periphery of the Rodian supercontinent (Li et al., 2008; Cawood et al., 2013; Cawood et al., 2017). Furthermore, the geologic setting of the Danzhou Group deposition remains controversial (Li et al., 1999; Wang and Li, 2003; Shu, 2012; Shu et al., 2014). Below, we discuss our new results and document the geological evolution of the eastern JO, creating a general tectonic evolution of the JO. We separated the tectonic history into four stages, with detailed descriptions as follows:

Stage 1: Paleoocean within the SCC during the Early Neoproterozoic

The mafic–ultramafic rocks from the Yuanbaoshan region in the southwestern JO in the SCC were emplaced in an arc or MORB setting ca. 861–834 Ma (Chen et al., 2014; Lin et al., 2015). Meso– and Neoproterozoic mafic–ultramafic rocks from the southwestern JO have mainly calc–alkaline features and display geochemical signatures of island arc volcanics. Hence, these mafic–ultramafic rocks are thought to be the products of magmatism at a convergent plate boundary (Zhou et al., 2004). To the northeastern part of the JO, mafic–ultramafic rocks existed from 1000 to 830 Ma. An approximately 970 Ma ridge subduction–related adakites, ~930 Ma Nb–enriched basalts (Zhang et al., 2015a, b), ~990–900 Ma arc–back–arc systems (Wang et al., 2015b), and ~871–835 Ma arc andesite and basalt (Wang et al., 2014; Yao et al., 2015a; Zhang et al., 2015b; Zhang and Wang, 2016) have been previously documented. Furthermore, a back–arc basin developed across the entire JO between 850 and 810 Ma (Li et al., 2016b).

Apart from ocean–related magmatism, there were two main subduction–related metamorphic stages in the JO. One period of amphibolite facies metamorphism occurred between 942 and 935 Ma and represents the time of the collision between the protocratonic Yangtze Block with the Rodinia supercontinent (Jiang et al., 2016). The other stage, between 912 and 835 Ma, was correlated to the collision of the Yangtze and Cathaysia Blocks (Yan et al., 2015).

These data indicate that a paleoocean was present between 1000 and 835 Ma in the JO inside the SCC and was significantly younger than the typical Grenvillian orogeny at 1.3–1.0 Ga (Wang et al., 2007). Therefore, the southeastern Yangtze Block was an active continental margin and cannot be placed in the center of the Rodinia supercontinent (Fig. 11a) (Wang et al., 2016). This interpretation precludes placing South China in central Rodinia. Instead, it was most likely situated in a marginal position, according to the paleomagnetic data (Yang et al., 2004).

Stage 2: Amalgamation of the Yangtze and Cathaysia Blocks during the Middle Neoproterozoic

A paleoocean, the precursor of the JO, was consumed by northwestward subduction beneath the Yangtze Block during the Neoproterozoic (980–850 Ma) (Yao et al., 2015a; Yao et al., 2016) (Fig. 11a). Remnants of the northwestern subduction zone are preserved as scattered (ultra)mafic blocks and mélanges of the Jiangnan sutures (Fig. 2) (Wang Jianguo et al., 2014a; Li et al., 2016c).

Near the Yuanbaoshan region, the Yangtze and the Cathaysia Blocks collided ca. 835–800 Ma, which led to the formation of the southwestern JO (Fig. 11b). This collisional event resulted in the syncollisional S–type Sangfang and Yuanbaoshan granite intrusion (Fig. 4) (Li, 1999; Yao et al., 2014c), which were subsequently exposed at the surface. In the central JO, the initial collision and final assemblage of the Yangtze with the Cathaysia Block was constrained to between 830 and 810 Ma, respectively (Zhang et al., 2015b; Guo et al., 2018).

There were voluminous ~820 Ma peraluminous granitoids in the JO in South China after the assembly of the Yangtze and Cathaysia Blocks (Wang et al., 2006; Zheng et al., 2008; Zhao et al., 2013). The geochemistry of the granitoids reveals typical S–type granite features. They formed in collision–related tectonic settings (Wang et al., 2006; Yao et al., 2014c). These conclusions indicate that the previously proposed ca. 980–880 Ma convergent plate margin setting in the eastern JO (Li et al., 2009) lasted until at least ~850 Ma (Cawood et al., 2013; Yao et al., 2015a), and constrains the final assembly of the Yangtze and Cathaysia Blocks to sometime between 850 and 810 Ma (e.g., Yao et al., 2016).

Stage 3: Intra–continental rifting stage inside the SCC

In the mapping area, the Lower Danzhou Group lies unconformably on the older Sibao Group and the exposed Yuansbaoshan granite and were deposited in an extensional basin related to the breakoff of a subducted

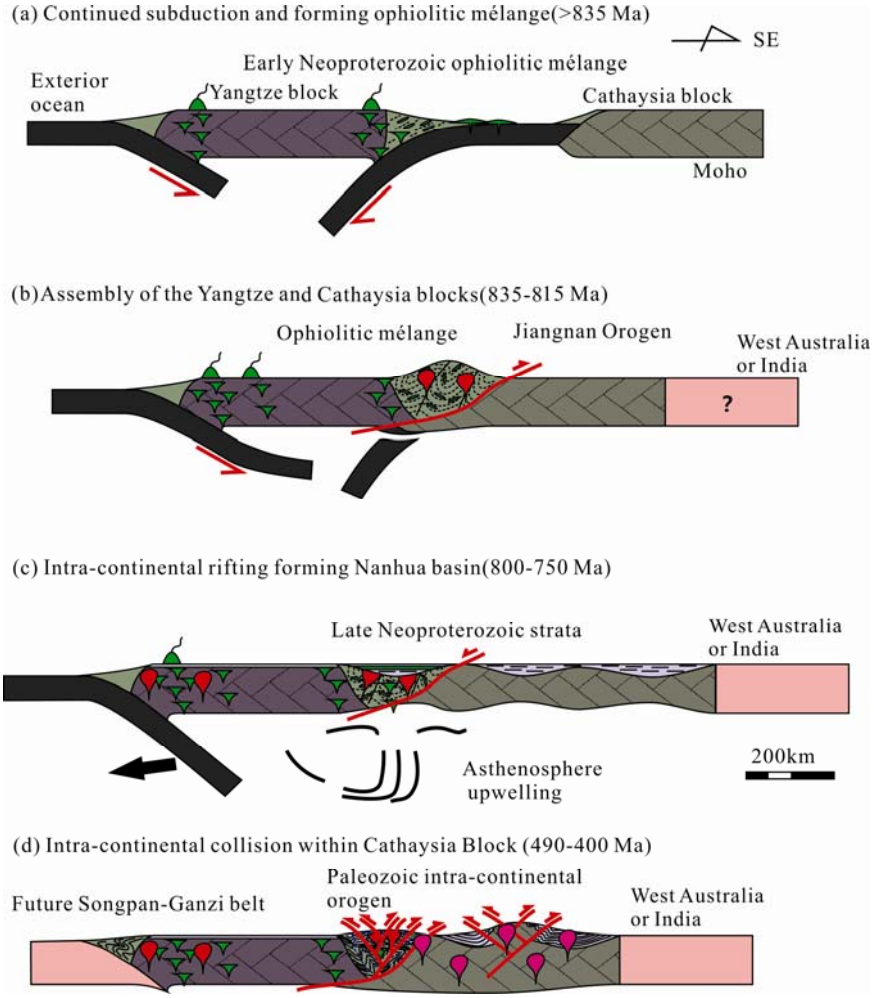


Fig. 11. Geodynamic evolutionary model of the Jiangnan Orogen within the SCC.
(a), >835 Ma, paleoocean evolution stage; (b), approximately 835–815 Ma, compressional stage, obduction of ophiolitic units and induced magmatism; (c), 800–750 Ma, intra–continental rifting stage and the formation of the Nanhua Basin; (d), approximately 490–400 Ma, transpression resulting in positive flower structures and synchronous exhumation of metamorphosed rocks and emplacement of granitoids.

oceanic slab (Fig. 11b) (Wang et al., 2006). Within the Danzhou Group, a volcanic layer dated, using the SHRIMP zircon U–Pb method, to between 814 Ma and 725 Ma (Lin et al., 2015; Gao Linzhi et al., 2015). It is possible that they were derived from an upwelling asthenosphere within a continental rifting environment (Zhou et al., 2007). Moreover, the Late Neoproterozoic strata show evidence of continuous extension and deposition in a rifting system (Wang and Li, 2003; Cui et al., 2015). Moreover, a synrift normal fault, the post–orogen Dexing–Huangshan normal fault zone, has been documented (Xu et al., 2014).

The unconformity in the central JO formed more or less synchronously throughout the orogen at 830–800 Ma, consistent with it dating the end of the collision between the Yangtze and Cathaysia Blocks (Cui et al., 2015). The A–type Daolinshan granite intrusion in the eastern JO is part of the magmatism associated with widespread rifting of the SCC approximately 790 Ma (Yao et al., 2014a). The mid–Neoproterozoic magmatic rocks in the JO formed in a post–orogenic extensional environment, based on a systematic geochronological and geochemical study on the 800–790 Ma igneous units (Wang et al., 2012a). The development of major rift basins that contain bimodal volcanic rocks may have continued until 690 Ma (Wang and Li, 2003). Such a long extensional event split the Cathaysia Block into several subblocks, and subsequently, several shallow sea basins developed in the regions between these subblocks (Shu, 2012). This extensional basin persisted until the Early Paleozoic with the absence of volcanic rocks and any evidence for input of mantle–derived components (Shu et al., 2015).

Stage 4: Intra–continental collision stage inside the SCC

The aforementioned data show that the Early Paleozoic orogeny in the Yuanbaoshan region was accommodated by (i) an east–directed deformation and weakly metamorphosed units located to the east of the Yuanbaohan granite and (ii) a west–directed deformation in the units located to the west of the Yuanbaoshan granite. The core of this different deformation area exhumed the highest metamorphic grade rocks in the study area and illustrates thick–skin tectonics. The more western area of the Sangfang granite only experienced thin–skinned tectonics that affected younger, low–grade (lower greenschist at maximum) meta–sediments over a décollement level (Yan et al., 2003). The inferred core of the ophiolitic mélange, structurally underlying the Danzhou Group in the western JO, represents remnants of a northwest dipping subduction–accretion complex.

In the Early Paleozoic, the rift environment of the SCC failed due to the intra–continental orogen (Shi et al., 2015; Yu et al., 2016). North–northeast–striking and east–west–dipping thrusts and reverse faults have been broadly recognized in the Yangtze Block and were attributed to the reactivated old suture zone faults (Charvet, 2013). The mélange sheet was obducted southeastward onto the northern margin of the Cathaysia terrane during the Neoproterozoic closure of the ocean. The new white mica ^{40}Ar–^{39}Ar ages range from 495 to 455 Ma, and are relatively older than the white mica $^{40}Ar/^{39}Ar$ ages of 393.2–419.4 Ma in the shear zone to the west of the Yuanbaoshan pluton (ZHANG Xuefeng, 2015).

Within the Cathasia Block, the Wuyishan area includes up to amphibolite facies metamorphism, which may also have been affected by thick–skinned tectonics and was responsible for crustal thickening between 465 and 400 Ma (Charvet et al., 2010; Shu et al., 2014; Xu et al., 2015; Zhang et al., 2016a). This metamorphic event was followed by anatexes and granitic intrusions mainly from 465 until 390 Ma (Yao et al., 2014b). The 435–415 Ma granitoids suggest that the Early Paleozoic plutons were derived from the partial melting of the Paleoproterozoic basement of the Cathaysia Block (Shu et al., 2015), indicating the Paleoproterozoic basement was involved in the tectonics (Charvet et al., 2010). Pre–existing block boundaries provide a proper location for the juxtaposition of asthenospheric upwelling and basaltic underplating during the collapse of an intra–continental orogen (Yu et al., 2016). A regional positive flower structural adds new constraints to the Paleozoic geological evolution of the SCC, which coincides with intra–continental orogen theory.

The Middle to Late Devonian angular unconformity and the thick coarse–grained clastic sequence provides additional evidence for an Early Paleozoic orogeny (Shu et al., 2015). During this orogeny, the Nanhua Basin changed from a mid–Neoproterozoic rift basin to a failed rift in the Late Neoproterozoic. This event was linked to a speculated diachronous collision between the SCC and northern India during the assembly of Gondwana (Yao et al., 2015b) or with Australia (Li et al., 2016a). An alternative idea proposed that the mid–Paleozoic orogen in the southeastern part of South China is an intra–continental orogenic event resulting from the propagation of compressive stresses related to the subduction of the Proto–Pacific Ocean along the margin of east Australia between 460 and 400 Ma (Han et al., 2015; Xu et al., 2016).

5.4 Subducted lithospheric interaction control evolution of the JO

The JO is a collisional belt that developed during the assembly of the SCC (Charvet et al., 2010; Zhao and

Cawood, 2012; Shu et al., 2015). The newly amalgamated SCC experienced rifting, starting approximately 800 Ma, marked by mafic–ultramafic magmatism until ~750 Ma (Gao Linzhi et al., 2015). The rifting sediments constitute siliciclastic deposits intercalated with abundant volcanic layers unconformably overlying the convergence–formed mélange.

Zhao et al. (2011) proposed an updated scenario for the slab–arc model, which suggests that the Yangtze Block had active continental arcs on its margins before ~830 Ma (Fig. 11a–c). After ~800 Ma, southeastward subduction along the western and northern margins of the Yangtze Block was still active, with slab bending and rollback resulting in asthenospheric upwelling, which led to the formation of the Nanhua Basin in response to the back–arc spreading and subsidence (Zhao et al., 2011). This model is supported by the duration of subduction around the margins of Rodinia, which precisely spans the time interval of lithospheric extension within the supercontinent that led to its breakup (Cawood et al., 2016).

During the Early Paleozoic, the tectonic framework of South China was mainly controlled by regional compression characterized by kilometer–scale folds and thrusts, the development of southeast–directed décollement shearing, amphibolite facies metamorphism and granitic plutons (Fig. 11d) (Faure et al., 2009; Charvet et al., 2010; Shu et al., 2015). These structural, metamorphic and magmatic features were related to the northwestward continental subduction of the southeastern part of the Neoproterozoic rift. The Nanhua Basin was closed and intra–continental collision occurred concomitantly. Most authors propose the far–field subducted plate force controlled this event (Han et al., 2015; Yao et al., 2015b; Li et al., 2016a; Xu et al., 2016).

These two tectonic events, in particular, have the potential to provide insights into the relative roles of lithospheric plate interactions in controlling the periods of continental aggregation and dispersal. Together, these results imply that the Jiangnan suture zone represents a significant and long–lived lithospheric weakness that was preferentially reactivated during at least two episodes of tectonic activity in regional far–field domains (Wang et al., 2015a).

6 Conclusions

Based on our structural and (thermo)geochronological results in the Yuanbaoshan region, integrated with the regional geology, we briefly summarized the Neoproterozoic to Early Paleozoic tectonic evolution of the Jiangnan Orogen and reached the following conclusions:

(1) The Sibao Group is younger than the maximum depositional age of ~835 Ma, which encloses the 1000–850 Ma oceanic affinity (ultra)mafic blocks that are a typical subduction mélange trait. These observations support the existence of an intervening oceanic lithosphere between the Yangtze and Cathaysia Blocks.

(2) Concomitantly after the consumption of an intervening oceanic domain between the Yangzte and Cathaysia Blocks, the Jiangnan Orogen was formed by the collision of these two blocks. The subsequent collision began ~835 Ma and was followed by late– to post–collisional granitic intrusions. The newly amalgamated South China Craton experienced exhumation, which exposed the ~815 Ma pluton on the surface.

(3) The united SCC experienced rifting, starting ~800 Ma, which allowed the Danzhou Group to be unconformably overlain on the Sibao Group and Yuanaoshan granite. This intra–continental extensional event formed the Nanhua rift basin and was marked by mafic–ultramafic magmatism until ~750 Ma.

(4) The Nanhua rift basin finally closed by the Early Paleozoic orogeny within the SCC. The Paleozoic orogeny was characterized by strong quasi–symmetrical intra–continental shortening and formed a positive flower structure in the Yuanbaoshan area, leading to crustal thickening. The Paleozoic orogenic event also exhumed metamorphosed rocks, which record a ca. 450 Ma cooling age.

(5) Our new geochronology results indicate that the South China Craton was located on the periphery of the Rodinia supercontinent during the Neoproterozoic and was connected to the Indian and northwest Australian continents during the Cambrian. A comparison of the tectonic evolution between the northeastern sections and the southeast section of the Jiangnan Orogen allow us to delineate a suture through the Yuanbaoshan area. It appears that either in situ or far–field subduction–related forces dominated the tectonic evolution of the South China Craton.

Acknowledgements

Here we really appreciate Prof. L.S. Shu, who has guided us during incipient field work and introduced regional geology comprehensively. This research is financially supported by Post–doctoral Scientific Foundation of China (No. 2016M601084), Basic research funds of the Chinese Academy of Geological Sciences (No.JYYWF20182103), Geological Survey of China (No.DD20160022–01) and a grant from the Ministry of Land and Resources of China (No. 201511022).

Manuscript received May 4, 2018
accepted June 21, 2018
edited by Fei Hongcai

References

BGMRGX (Bureau of Geology and Mineral Resources of Guangxi Zhuang Autonomous Region), 1966. *1:200,000 Geology map of Sanjiang Region* (in Chinese).

BGMRGX (Bureau of Geology and Mineral Resources of Guangxi Zhuang Autonomous Region), 1967. *1:200,000 Geology map of RonganRegion* (in Chinese).

BGMRGX (Bureau of Geology and Mineral Resources of Guangxi Zhuang Autonomous Region), 1969. *1:200,000 Geology map of Luocheng Region* (in Chinese).

BGMRGZ (Bureau of Geology and Mineral Resources of Guizhou Province), 1965. *1:200,000 Geology map of Rongjiang Region* (in Chinese).

Boger, S.D., Wilson, C.J.L., and Fanning, C.M., 2001. Early Paleozoic tectonism within the East Antarctic craton: The final suture between east and west Gondwana? *Geology*, 29: 463–466.

Bruguier, O., Lancelot, J., and Malavieille, J., 1997. U–Pb dating on single detrital zircon grains from the Triassic Songpan–Ganze flysch (Central China): Provenance and tectonic correlations. *Earth and Planetary Science Letters,* 152:217–231.

Cawood, P.A.,and Buchan, C., 2007. Linking accretionary orogenesis with supercontinent assembly. *Earth-Science Reviews*, 82: 217–256.

Cawood, P.A., Hawkesworth, C., and Dhuime, B., 2012. Detrital zircon record and tectonic setting. *Geology*, 40:875–878.

Cawood, P.A., Strachan, R.A., Pisarevsky, S.A., Gladkochub, D.P., and Murphy, J.B., 2016. Linking collisional and accretionary orogens during Rodinia assembly and breakup: Implications for models of supercontinent cycles. *Earth and Planetary Science Letters,* 449: 118–126.

Cawood, P.A., Wang, Y., Xu, Y., and Zhao, G., 2013. Locating South China in Rodinia and Gondwana: A fragment of greater India lithosphere? *Geology,* 41: 903–906.

Cawood, P.A., Zhao, G., Yao, J., Wang, W., Xu, Y., and Wang, Y., 2017. Reconstructing South China in Phanerozoic and Precambrian supercontinents. *Earth–Science Reviews* (in press).

Charvet, J., 2013. The Neoproterozoic–early Paleozoic tectonic evolution of the South China Block: an overview. *Journal of Asian Earth Sciences*, 74: 198–209.

Charvet, J., Shu, L., Faure, M., Choulet, F., Wang, B., Lu, H., and Le Breton, N., 2010. Structural development of the Lower Paleozoic belt of South China: genesis of an intracontinental orogen. *Journal of Asian Earth Sciences,* 39: 309–330.

Chen, Q., Sun, M., Long, X., Zhao, G., and Yuan, C., 2016. U–Pb ages and Hf isotopic record of zircons from the late Neoproterozoic and Silurian–Devonian sedimentary rocks of the western Yangtze Block: Implications for its tectonic evolution and continental affinity. *Gondwana Research*, 31: 184–199.

Chen, X., Wang, D., Wang, X.L., Gao, J.F., Shu, X.J., Zhou, J.C., and Qi, L., 2014. Neoproterozoic chromite–bearing high–Mg diorites in the western part of the Jiangnan orogen, southern China: Geochemistry, petrogenesis and tectonic implications. *Lithos*, 200–201: 35–48.

Collins, A.S., and Pisarevsky, S.A., 2005. Amalgamating eastern Gondwana: The evolution of the Circum–Indian Orogens. *Earth–Science Reviews*, 71: 229–270.

Cui, X., Zhu, W., Fitzsimons, I., He, J., Lu, Y., Wang, X., Ge, R., Zheng, B., and Wu, X., 2015. U–Pb age and Hf isotope composition of detrital zircons from Neoproterozoic sedimentary units in southern Anhui Province, South China: Implications for the provenance, tectonic evolution and glacial history of the eastern Jiangnan Orogen. *Precambrian Research*, 271: 65–82.

Dickinson, W.R., and Gehrels, G.E., 2009. Use of U–Pb ages of detrital zircons to infer maximum depositional ages of strata: a test against a Colorado Plateau Mesozoic database. *Earth and Planetary Science Letters*, 288: 115–125.

Dong, S., Zhang, Y., Gao, R., Su, J., Liu, M., and Li, J., 2015. A possible buried Paleoproterozoic collisional orogen beneath central South China: Evidence from seismic–reflection profiling. *Precambrian research*, 264: 1–10.

Faure, M., Lin, W., Chu, Y., and Lepvrier, C., 2016. Triassic tectonics of the southern margin of the South China Block. *Comptes Rendus Geoscience*, 348: 5–14.

Faure, M., Shu, L., Wang, B., Charvet, J., Choulet, F., and Monié, P., 2009. Intracontinental subduction: a possible mechanism for the Early Palaeozoic Orogen of SE China. *Terra Nova*, 21: 360–368.

Fergusson, C.L., Henerson, R.A., Fanning, C.M., and Withnall, I.W., 2007. Detrital zircon ages in Neoproterozoic to Ordovician siliciclastic rocks, northeastern Australia: implications for the tectonic history of the East Gondwana continental margin. *Journal of the Geological Society*, 164: 215–225.

Fitzsimons, and I.C.W., 2000. Grenville–age basement provinces in East Antarctica: Evidence for three separate collisional orogens. *Geology*, 28: 879–882.

Gao, Linzhi, Yin, Chunyu, Ding, Xiaozhong, Wang, Zejiu and Zhang, Heng., 2015. Rating Data of the Neoproterozoic Chronostratigraphy and Stratigraphic Correlation in South China. *Acta Geoscientica Sinica,* 36(5): 533–545 (in Chinese with English abstract).

Gaidies, F., Petley–Ragan, A., Chakraborty, S., Dasgupta, S., and Jones, P., 2015. Constraining the conditions of Barrovian metamorphism in Sikkim, India: P–T–t paths of garnet crystallization in the Lesser Himalayan Belt. *Journal of Metamorphic Geology*, 33: 23–44.

Griffin, W.L., Belousova, E.A., Shee, S.R., Pearson, N.J., and O'Reilly, S.Y., 2004. Archean crustal evolution in the northern Yilgarn Craton: U–Pb and Hf–isotope evidence from detrital zircons. *Precambrian Research*, 131: 231–282.

Guo, F., Shi, G., Yang, Q., Zhang, W., Xie, C., Zhou, W., and Zhang, J., 2018. Timing of metamorphism and provenance of the metamorphic basement of the Xiangshan uranium orefield, Jiangxi Province, China. *Acta Geologica Sinica* (English Edition), 92(1): 34–55.

Han, Z., Yang, Z., Tong, Y., and Jing, X., 2015. New paleomagnetic results from Late Ordovician rocks of the Yangtze Block, South China, and their paleogeographic implications. *Journal of Geophysical Research: Solid Earth*, 120: 4759–4772.

Harrison, T.M., Célérier, J., Aikman, A.B., Hermann, J., and Heizler, M.T., 2009. Diffusion of 40Ar in muscovite.

Geochimica et Cosmochimica Acta, 73: 1039–1051.

Jiang, X., Peng, S., Polat, A., Kusky, T., Wang, L., Wu, T., Lin, M., and Han, Q., 2016. Geochemistry and geochronology of mylonitic metasedimentary rocks associated with the Proterozoic Miaowan Ophiolite Complex, Yangtze craton, China: Implications for geodynamic events. *Precambrian Research*, 279: 37–56.

Li, J., Dong, S., Zhang, Y., Zhao, G., Johnston, S.T., Cui, J., and Xin, Y., 2016a. New insights into Phanerozoic tectonics of south China: Part 1, polyphase deformation in the Jiuling and Lianyunshan domains of the central Jiangnan Orogen. *Journal of Geophysical Research: Solid Earth*, 121: 3048–3080.

Li, J., Shi, W., Zhang, Y., Dong, S., and Ma, Z., 2016. Thermal evolution of the Hengshan extensional dome in central South China and its tectonic implications: New insights into low–angle detachment formation. *Gondwana Research*, 35: 425–441.

Li, L., Lin, S., Xing, G., Davis, D.W., Jiang, Y., Davis, W., and Zhang, Y., 2016b. Ca. 830 Ma back–arc type volcanic rocks in the eastern part of the Jiangnan orogen: Implications for the Neoproterozoic tectonic evolution of South China Block. *Precambrian Research*, 275: 209–224.

Li, X.H., Li, W.X., Li, Z.X., Lo, C.H., Wang, J., Ye, M.F., and Yang, Y.H., 2009. Amalgamation between the Yangtze and Cathaysia Blocks in South China: constraints from SHRIMP U–Pb zircon ages, geochemistry and Nd–Hf isotopes of the Shuangxiwu volcanic rocks. *Precambrian Research*, 174: 117–128.

Li, X., Zheng, J., Li, S., Liu, B., Xiang, L., Wang, Y., and Liu, X., 2016c. Late Triassic orogenic collapse and Palaeo‐Pacific slab roll‐back beneath central South China: constraints from mafic granulite xenoliths and structural features. *Geological Journal*, 51: 123–136.

Li, X.H., 1999. U–Pb zircon ages of granites from the southern margin of the Yangtze Block: timing of Neoproterozoic Jinning: Orogeny in SE China and implications for Rodinia Assembly. *Precambrian Research,* 97:43–57.

Li, Z.X., Bogdanova, S., Collins, A., Davidson, A., De Waele, B., Ernst, R., Fitzsimons, I., Fuck, R., Gladkochub, D., and Jacobs, J., 2008. Assembly, configuration, and break–up history of Rodinia: a synthesis. *Precambrian research*, 160: 179–210.

Li, Z.X., Li, X.H., Zhou, H., and Kinny, P.D., 2002. Grenvillian continental collision in south China: New SHRIMP U–Pb zircon results and implications for the configuration of Rodinia. *Geology*, 30: 163–166.

Li, Z.X., Li, X., Kinny, P., Wang, J., Zhang, S., and Zhou, H., 2003. Geochronology of Neoproterozoic syn–rift magmatism in the Yangtze Craton, South China and correlations with other continents: evidence for a mantle superplume that broke up Rodinia. *Precambrian Research*, 122: 85–109.

Li, Z., Li, X., Kinny, P., and Wang, J., 1999. The breakup of Rodinia: did it start with a mantle plume beneath South China? *Earth and Planetary Science Letters*, 173: 171–181.

Lin, M., Peng, S., Jiang, X., Polat, A., Kusky, T., Wang, Q., and Deng, H., 2015. Geochemistry, petrogenesis and tectonic setting of Neoproterozoic mafic–ultramafic rocks from the western Jiangnan orogen, South China. *Gondwana Research*, 35: 338–356.

Liu, Y.S., Hu, Z.C., Zong, K.Q., Gao, C.G., Gao, S., Xu, J., and Chen, H.H., 2010. Reappraisement and refinement of zircon U–Pb isotope and trace element analyses by LA–ICP–MS. *Chinese Science Bulletin* (English Edition), 55: 1535–1546.

Ludwig, K.R., 2001. Isoplot/Ex, rev.2.49: a geochronological toolkit for Microsoft Excel. *Berkeley Geochronoly Center Specical Publication* (1a): 55.

Ma, X., Yang, K., Li, X., Dai, C., Zhang, H., and Zhou, Q., 2016. Neoproterozoic Jiangnan Orogeny in Southeast Guizhou, South China: Evidence from U–Pb ages for Detrital Zircons from the Sibao Group and Xiajiang Group. *Canadian Journal of Earth Sciences*, 53: 219–230.

Myrow, P.M., Hughes, N.C., Goodge, J.W., Fanning, C.M., Williams, I.S., Peng, S., Bhargava, O.N., Parcha, S.K.,and Pogue, K.R., 2010. Extraordinary transport and mixing of sediment across Himalayan central Gondwana during the Cambrian–Ordovician. *Geological Society of America Bulletin*, 122: 1660–1670.

Nance, R.D., Murphy, J.B., and Santosh, M., 2014. The supercontinent cycle: A retrospective essay. *Gondwana Research,* 25:4–29.

Shi, W., Dong, S., Zhang, Y., and Huang, S., 2015. The typical large–scale superposed folds in the central South China: Implications for Mesozoic intracontinental deformation of the South China Block. *Tectonophysics*, 664: 50–66.

Shu, L.S., 2012. An analysis of principal features of tectonic evolution in South China Block. *Geological Bulletin of China* (English Edition), 31(7): 1035–1053.

Shu, L., Wang, B., Cawood, P.A., Santosh, M., and Xu, Z., 2015. Early Paleozoic and Early Mesozoic intraplate tectonic and magmatic events in the Cathaysia Block, South China. *Tectonics,* 34: 1600–1621.

Shu, L.S., Jahn, B.M., Charvet, J., Santosh, M., Wang, B., Xu, X., and Jiang, S., 2014. Early Paleozoic depositional environment and intraplate tectono–magmatism in the Cathaysia Block (South China): Evidence from stratigraphic, structural, geochemical and geochronological investigations. *American Journal of Science*, 314: 154–186.

Wang, D., Wang, X.L., Zhou, J.C., and Shu, X.J., 2013a. Unraveling the Precambrian crustal evolution by Neoproterozoic conglomerates, Jiangnan orogen: U–Pb and Hf isotopes of detrital zircons. *Precambrian Research*, 233: 223–236.

Wang, F., Chen, H., Batt, G.E., Lin, X., Gong, J., Gong, G., Meng, L., Yang, S., and Jourdan, F., 2015a. Tectonothermal history of the NE Jiangshan–Shaoxing suture zone: Evidence from $^{40}Ar/^{39}Ar$ and fission–track thermochronology in the Chencai region. *Precambrian Research,* 264: 192–203.

Wang, J., and Li, Z.X., 2003. History of Neoproterozoic rift basins in South China: implications for Rodinia break–up. *Precambrian Research*, 122: 141–158.

Wang Jianguo, Yu Shengqiang, Hu Yanhua, Zhao Xudong, Wu Ming and Gu Mingguang, 2014a. The discovery, petrology and geochronology of the retrograde eclogite in Jiangshan–Shaoxing suture zone. *Geology in China*, 41(4): 1356–1363 (in Chinese with English abstract).

Wang, L.J., Griffin, W.L., Yu, J.H., and O'Reilly, S.Y., 2010. Precambrian crustal evolution of the Yangtze Block tracked by detrital zircons from Neoproterozoic sedimentary rocks. *Precambrian Research,*177:131–144.

Wang Sungshan, 1983. Age determinations of $^{40}Ar–^{40}K$, $^{40}Ar–^{39}Ar$ and radiogenic ^{40}Ar released characteristics on K–Ar geostandards of China. *Chinese Journal of Geology*, 4: 315–

323 (in Chinese with English abstract).

Wang, W., Zhao, J.H., Zhou, M.F., Yang, S.H., and Chen, F.K., 2014b. Neoproterozoic mafic–ultramafic intrusions from the Fanjingshan region, South China: Implications for subduction –related magmatism in the Jiangnan fold belt. *The Journal of Geology*, 122: 455–473.

Wang, W., Zhou, M.F., Zhao, J.H., Pandit, M.K., Zheng, J.P., and Liu, Z.R., 2016. Neoproterozoic active continental margin in the southeastern Yangtze Block of South China: Evidence from the ca. 830–810 Ma sedimentary strata. *Sedimentary Geology*, 342: 254–267.

Wang, X.C., Li, Z.X., Li, X.H., Li, Q.L., Tang, G.Q., Zhang, Q.R., and Liu, Y., 2011. Nonglacial origin for low–δ18O Neoproterozoic magmas in the South China Block: Evidence from new in–situ oxygen isotope analyses using SIMS. *Geology*, 39: 735–738.

Wang, X.L., Shu, L.S., Xing, G.F., Zhou, J.C., Tang, M., Shu, X.J., Qi, L.,and Hu, Y.H., 2012a. Post–orogenic extension in the eastern part of the Jiangnan orogen: Evidence from ca 800 –760 Ma volcanic rocks. *Precambrian Research,* 222–223: 404–423.

Wang, X.L., Zhou, J.C., Griffin, W.a., Wang, R.C., Qiu, J.S., O'Reilly, S., Xu, X., Liu, X.M.,and Zhang, G.L., 2007. Detrital zircon geochronology of Precambrian basement sequences in the Jiangnan orogen: dating the assembly of the Yangtze and Cathaysia Blocks. *Precambrian Research*, 159: 117–131.

Wang, X.L., Zhou, J.C., Qiu, J.S., Zhang, W.L., Liu, X.M., and Zhang, G.L., 2006. LA–ICP–MS U–Pb zircon geochronology of the Neoproterozoic igneous rocks from Northern Guangxi, South China: Implications for tectonic evolution. *Precambrian Research*, 145: 111–130.

Wang, X.S., Gao, J., Klemd, R., Jiang, T., Zhai, Q.G., Xiao, X.C.,and Liang, X.Q., 2015b. Early Neoproterozoic multiple arc–back–arc system formation during subduction–accretion processes between the Yangtze and Cathaysia blocks: New constraints from the supra–subduction zone NE Jiangxi ophiolite (South China). *Lithos*, 236: 90–105.

Wang, Y., Fan, W., Zhang, G., and Zhang, Y., 2013b. Phanerozoic tectonics of the South China Block: key observations and controversies. *Gondwana Research*, 23:1273–1305.

Wang, Y., Wu, C., Zhang, A., Fan, W., Zhang, Y., Zhang, Y., Peng, T., and Yin, C., 2012b. Kwangsian and Indosinian reworking of the eastern South China Block: constraints on zircon U–Pb geochronology and metamorphism of amphibolites and granulites. *Lithos*, 150: 227–242.

Wang, Z., Wang, J., Du, Q., Deng, Q., Yang, F., and Wu, H., 2013c. Mature Archean continental crust in the Yangtze craton: Evidence from petrology, geochronology and geochemistry. *Chinese Science Bulletin* (English Edition), 58: 2360–2369.

Xu, X., Li, Y., Tang, S., Xue, D., and Zhang, Z., 2015. Neoproterozoic to Early Paleozoic polyorogenic deformation in the southeastern margin of the Yangtze Block: Constraints from structural analysis and 40 Ar/39 Ar geochronology. *Journal of Asian Earth Sciences*, 98: 141–151.

Xu, X., Xue, D., Li, Y., Hu, P., and Chen, N., 2014. Neoproterozoic sequences along the Dexing–Huangshan fault zone in the eastern Jiangnan orogen, South China: geochronological and geochemical constrains. *Gondwana Research*, 25: 368–382.

Xu, Y.J., Cawood, P.A., and Du, Y.S., 2016. Intraplate orogenesis in response to Gondwana assembly: Kwangsian Orogeny, South China. *American Journal of Science*, 316: 329–362.

Xu, Y., Cawood, P.A., Du, Y., Hu, L., Yu, W., Zhu, Y., and Li, W., 2013. Lingking south China to northern Australia and India on the margin of Gondwana: Constraints from detrital zircon U–Pb and Hf isotopes in Cambrian strata. *Tectonics*, 32: 1547–1558.

Xun, Z., Allen, M.B., Whitham, A.G., and Price, S.P., 1996. Rift–related Devonian sedimentation and basin development in South China. *Journal of Southeast Asian Earth Sciences*, 14: 37–52.

Yan, C., Shu, L., Michel, F., Chen, Y., and Li, C., 2017. Early Paleozoic intracontinental orogeny in the Yunkai domain, South China Block: New insights from field observations, zircon U–Pb geochronological and geochemical investigations. *Lithos*, 268–271: 320–333.

Yan, C., Shu, L., Santosh, M., Yao, J., Li, J., and Li, C., 2015. The Precambrian tectonic evolution of the western Jiangnan orogen and western Cathaysia Block: Evidence from detrital zircon age spectra and geochemistry of clastic rocks. *Precambrian Research*, 268: 33–60.

Yan, D.P., Zhou, M.F., Song, H.L., Wang, X.W., and Malpas, J., 2003. Origin and tectonic significance of a Mesozoic multi–layer over–thrust system within the Yangtze Block (South China). *Tectonophysics*, 361: 239–254.

Yang, C., Li, X.H., Wang, X.C., and Lan, Z., 2015. Mid–Neoproterozoic angular unconformity in the Yangtze Block revisited: Insights from detrital zircon U–Pb age and Hf–O isotopes. *Precambrian Research*, 266: 165–178.

Yang, Z., Sun, Z., Yang, T., and Pei, J., 2004. A long connection (750–380 Ma) between South China and Australia: paleomagnetic constraints. *Earth and Planetary Science Letters*, 220: 423–434.

Yao, J., Shu, L., Cawood, P.A., and Li, J., 2016. Delineating and characterizing the boundary of the Cathaysia Block and the Jiangnan orogenic belt in South China. *Precambrian Research*, 275: 265–277.

Yao, J., Shu, L., and Santosh, M., 2014a. Neoproterozoic arc–trench system and breakup of the South China Craton: Constraints from N–MORB type and arc–related mafic rocks, and anorogenic granite in the Jiangnan orogenic belt. *Precambrian Research*, 247: 187–207.

Yao, J., Shu, L., Santosh, M., and Li, J., 2015a. Neoproterozoic arc–related andesite and orogeny–related unconformity in the eastern Jiangnan orogenic belt: Constraints on the assembly of the Yangtze and Cathaysia blocks in South China. *Precambrian Research*, 262: 84–100.

Yao, J., Shu, L., Santosh, M., and Xu, Z., 2014b. Palaeozoic metamorphism of the Neoproterozoic basement in NE Cathaysia: zircon U–Pb ages, Hf isotope and whole–rock geochemistry from the Chencai Group. *Journal of the Geological Society*, 171: 281–297.

Yao, J., Shu, L., Santosh, M., and Zhao, G., 2014c. Neoproterozoic arc–related mafic–ultramafic rocks and syn–collision granite from the western segment of the Jiangnan Orogen, South China: constraints on the Neoproterozoic assembly of the Yangtze and Cathaysia Blocks. *Precambrian Research*, 243: 39–62.

Yao, W.H., Li, Z.X., Li, W.X., Su, L., and Yang, J.H., 2015b. Detrital provenance evolution of the Ediacaran–Silurian

Nanhua foreland basin, South China. *Gondwana Research*, 28: 1449–1465.

Yin, J., Chen, W., Xiao, W., Yuan, C., Sun, M., Tang, G., Yu, S., Long, X., Cai, K.,and Geng, H., 2015. Petrogenesis of Early–Permian sanukitoids from West Junggar, Northwest China: Implications for Late Paleozoic crustal growth in Central Asia. *Tectonophysics*, 662: 385–397.

Yu, Y., Huang, X.L., He, P.L.,and Li, J., 2016. I–type granitoids associated with the early Paleozoic intracontinental orogenic collapse along pre–existing block boundary in South China. *Lithos*, 248: 353–365.

Zhai, M., 2015. *Precambrian Geology of China*. Springer.

Zhang, Xuefeng, 2015. Research on the Sibao ductile shear zone, northern Guangxi. A dissertation from China University of Geosciences for doctoral degree (in Chinese with English abstract).

Zhang, C.L., Zou, H.B., Zhu, Q.B., and Chen, X.Y., 2015a. Late Mesoproterozoic to early Neoproterozoic ridge subduction along southern margin of the Jiangnan Orogen: New evidence from the Northeastern Jiangxi Ophiolite (NJO), South China. *Precambrian Research*, 268: 1–15.

Zhang, C., Yu, J., O'Reilly, S., Griffin, W., Qian, J., Liu, Q., Lou, F., Zhou, X., and Shen, L., 2016a. Granulite facies xenoliths from the Yuhuashan complex, central Jiangxi, South China: constraints on Late Palaeozoic orogeny and middle‐lower crust components. *Journal of Metamorphic Geology*, 34: 45–61.

Zhang Shitao, Ma Dongsheng, Lu Jianjun, Zhang Rongqing, Cai Yang and Ding Chaochao, 2016c, Geochronology, Hf isotopic compositions and geochemical characteristics of the Pingying granite pluton in northern Guangxi, South China, and its geological significance. *Geological Journal of China Universities*, 22: 092–104 (in Chinese with English abstract).

Zhang, H., Tingdong, L.I., Ying, X., Zhang, C., Gao, L., Geng, S., and Chen, T., 2015b. Geochronology and tectonic evolution of the west section of the Jiangnan orogenic belt. *Acta Geologica Sinica* (English Edition), 89(5): 1497–1515.

Zhang, J., Fan, T., Algeo, T.J., Li, Y., and Zhang, J., 2016b. Paleo–marine environments of the early Cambrian Yangtze Platform. *Palaeogeography*, *Palaeoclimatology*, *Palaeoecology*, 443: 66–79.

Zhang, Y., and Wang, Y., 2016. Early Neoproterozoic (~840 Ma) arc magmatism: Geochronological and geochemical constraints on the metabasites in the Central Jiangnan Orogen. *Precambrian Research*, 275: 1–17.

Zhang, Y., Wang, Y., Zhang, Y., and Zhang, A., 2015b. Neoproterozoic assembly of the Yangtze and Cathaysia blocks: Evidence from the Cangshuipu Group and associated rocks along the Central Jiangnan Orogen, South China. *Precambrian Research*, 269: 18–30.

Zhao, G., 2015. Jiangnan Orogen in South China: developing from divergent double subduction. *Gondwana Research*, 27: 1173–1180.

Zhao, G., and Cawood, P.A., 2012. Precambrian geology of China. *Precambrian Research,* 222: 13–54.

Zhao, J.H., Zhou, M.F., Yan, D.P., Zheng, J.P., and Li, J.W., 2011. Reappraisal of the ages of Neoproterozoic strata in South China: no connection with the Grenvillian orogeny. *Geology*, 39: 299–302.

Zhao, J.H., Zhou, M.F., and Zheng, J.P., 2013. Constraints from zircon U–Pb ages, O and Hf isotopic compositions on the origin of Neoproterozoic peraluminous granitoids from the Jiangnan Fold Belt, South China. *Contributions to Mineralogy and Petrology*, 166: 1505–1519.

Zheng, Y.F., Wu, R.X., Wu, Y.B., Zhang, S.B., Yuan, H., and Wu, F.Y., 2008. Rift melting of juvenile arc–derived crust: geochemical evidence from Neoproterozoic volcanic and granitic rocks in the Jiangnan Orogen, South China. *Precambrian Research*, 163: 351–383.

Zheng, Y.F., Zhang, S.B., Zhao, Z.F., Wu, Y.B., Li, X., Li, Z., and Wu, F.Y., 2007. Contrasting zircon Hf and O isotopes in the two episodes of Neoproterozoic granitoids in South China: implications for growth and reworking of continental crust. *Lithos*, 96: 127–150.

Zhou, J., Li, X.H., Ge, W., Li, and Z.X., 2007. Age and origin of middle Neoproterozoic mafic magmatism in southern Yangtze Block and relevance to the break–up of Rodinia. *Gondwana Research*, 12: 184–197.

Zhou, J., Wang, X., Qiu, J., and Gao, J., 2004. Geochemistry of Meso–and Neoproterozoic mafic–ultramafic rocks from northern Guangxi, China: Arc or plume magmatism? *Geochemical Journal*, 38: 139–152.

Zhou, M.F., Ma, Y., Yan, D.P., Xia, X., Zhao, J.H., and Sun, M., 2006. The Yanbian terrane (Southern Sichuan Province, SW China): a Neoproterozoic arc assemblage in the western margin of the Yangtze block. *Precambrian Research*, 144: 19–38.

Zhou, M.F., Yan, D.P., Kennedy, A.K., Li, Y., and Ding, J., 2002. SHRIMP U–Pb zircon geochronological and geochemical evidence for Neoproterozoic arc–magmatism along the western margin of the Yangtze Block, South China. *Earth and Planetary Science Letters*, 196: 51–67.

About the first author

ZHAO Zhongbao: Male, born in 1985 in Shanxi Province; Graduated from Tuebingen University, Germany. Doctor ZHAO Zhongbao is currently a postdoctor at the Institute of Geology, Chinese Academy of Geological Science. His current research interest focuses on the structural evolution in the old suture zone and orogenic belt. Email:zhaozhb04@163.com; phone:15811039081; Personal ID: 142431198507250910.

Cover Illustrator

Picture in the top left corner: the upper left is the small tightly closed folds in the Neoproterozoic Danzhou group in the northern Guangxi.

Picture in the top right corner: the upper right is the complex superimposed folds in the Neoproterozoic Sibao Group in the northern Guangxi.

Picture in the lower left corner: the lower left is the upright tight folds developed in the Danzhou Group in Longsheng area, Guangxi.

Picture in the lower right corner: the lower right shows that the Late Neoproterozoic Danzhou mudstone thrusted eastward onto the Cambrian limestone in the northern Guangxi.